The effect of depleting the CNS Border associated macrophages at pre-symptomatic stage of ALS on neuroinflammation, symptoms, and survival

By

Narges SHOMALIZADEH

A Dissertation Submitted to the

Graduate School of Health Sciences in Partial Fulfillment of the Requirements for the Degree of

Doctor of Philosophy

in

Neuroscience

KOÇ ÜNİVERSİTESİ

February , 2024

The effect of depleting the CNS Border associated macrophages at pre-symptomatic stage of ALS on neuroinflammation, symptoms, and survival

Koc University

Graduate School of Health Sciences

This is to certify that I have examined this copy of a doctoral dissertation by

Narges SHOMALIZADEH

and have found that it is complete and satisfactory in all respects,

and that any and all revisions required by the final

examining committee have been made.

Committee Members:

Prof. Dr. Yasemin Gürsoy Özdemir (Advisor)

Dr. Sebastian A. Lewandowski

Assoc. Prof. Dr Atay Vural

Prof. Dr. Mehmet Kaya

Prof. Dr. Erdem Tüzün

Date: 05.02.2024

"Dedicated to my father, who was a victim of ALS.

His memories will never leave me.".

ABSTRACT

The effect of depleting the CNS Border associated macrophages at pre-symptomatic stage of ALS on neuroinflammation, symptoms, and survival

Narges SHOMALIZADEH

Doctor of Philosophy in Neuroscience, February 2023

Background: Amyotrophic lateral sclerosis (ALS) is an incurable motor neuron disease characterized by progressive muscle atrophy, including respiratory muscles. Muscle weakness, wasting, cramps, and fasciculations result from the loss of lower motor neurons. Additionally, patients with ALS may experience extra-motor symptoms due to neuronal loss in the frontotemporal cortex. Survival typically ranges from 2 to 4 years after disease onset, with respiratory failure being the primary cause of death. ALS, the most common motor neuron disease in adults, has an incidence of 2 per 100,000 and a prevalence of 5.4 per 100,000. Despite extensive studies on ALS pathogenesis, the exact mechanism of neurodegeneration remains unclear.

Perivascular macrophages (PVMs) are myeloid cells residing in the central nervous system (CNS) and are part of the larger group of macrophages known as CNS border-associated macrophages. In a healthy state, these cells phagocytize harmful substances that infiltrate from the vasculature and regulate immune responses. However, in an inflammatory state, they contribute to increased vascular permeability and subsequent neuroinflammation. Dysregulation of the blood-brain barrier (BBB) occurs well before the symptomatic stage of ALS and influences PVMs, leading to increased reactive oxygen species (ROS) generation and BBB permeability. Transformed PVMs, in collaboration with other brain myeloid cells, initiate proinflammatory processes.

Aim: Our aim is to investigate the contribution of PVMs to ALS pathogenesis and their impact on neuroinflammation. To achieve this, we depleted PVMs at the presymptomatic stage of ALS and evaluated microglia activation, astrogliosis, BBB disruption, symptoms, and lifespan in an animal model.

Methods: PVM depletion was achieved by injecting clodronate-loaded liposomes or PBS-loaded liposomes (as a control) into the cisterna magna of SOD1$^{(G93A)}$ mutated rats, an ALS animal model. The study included 59 SOD1 mutated rats (both male and female). Preliminary studies involved nine rats, while the remaining fifty rats received either clodronate-loaded liposomes (depleted group) or PBS-loaded liposomes (sham group) via cisternal injection. The clodronate concentration in the suspension was 5 mg/ml. Rats were divided into three experiments: early single injection (day 80 after birth), late single injection (day 160 after birth), and multiple injections (administered at day 80 after birth followed by two additional injections every 20 days). Rats were monitored until reaching the humane endpoint, when the rats cannot turn back after being placed on their side, with weight measured twice a week and locomotor activity tested weekly to assess neuromuscular strength, motor coordination, and balance. The locomotor activity test comprised gait analysis, tail elevation, balance beam test, paw-grip endurance, extension reflex, rearing behavior, and ladder rung test for paw placement accuracy during walking.

Validation studies included wild-type (WT) rats from a Sprague Dawley background for comparison of PVMs between SOD1 and WT rats, injection point validation, and confirmation of PVM depletion. FITC-Albumin injection into the cisterna magna of two WT rats confirmed appropriate delivery to the brain and spinal cord.

Immunofluorescent staining of astrocytes, microglia, and CD206^{+} cells in obtained tissues from sacrificed animal models was conducted using GFAP, Iba 1, and CD206 primary antibodies, respectively. Statistical methods were employed to analyze behavior scoring and weight change, as well as staining results, between depleted and sham groups in the three experiments.

Results: Preliminary studies on CNS tissues from SOD1 and WT rats revealed upregulation of CD206^{+} cells in various brain and spinal cord regions of SOD1 mutated rats.

FITC-Albumin injection confirmed delivery to the brain and spinal cord, colocalizing with PVMs, validating the injection point for subsequent studies.

Immunofluorescence staining with CD206 for brain and spinal cord sections of WT rats showed downregulation of CD206^{+} cells in all regions of the depleted group, with significant results for the spinal cord in the multiple injection experiment.

Weight change analysis indicated a delayed presymptomatic stage in the depleted group across all three experiments, with significant results for the multiple injection experiment. Behavioral studies confirmed milder or delayed symptomatic stages in the depleted groups, particularly in the multiple injection experiment.

Immunofluorescence staining for PVMs, astrocytes, and microglia revealed upregulation of all three cell types in the ventral horn of the lumbar section of the spinal cord in the depleted group compared to the sham group in both the late single injection and multiple injection experiments.

Conclusion: This study demonstrated that depleting perivascular macrophages at the presymptomatic stage of ALS can delay disease onset, particularly in animals receiving repetitive doses of clodronate-loaded liposomes. Locomotor activity tests and weight change records showed a delayed and milder symptomatic phase in these animals. The upregulation of $CD206^+$ cells, microglia, and astrocytes at the endpoint in the ventral horn of the depleted group appears to be associated with the anti-inflammatory phenotype of $CD206^+$ cells, astrocytes, and microglia, correlating with improved motor behavior in this group.

Key words: Perivascular macrophages, Clodronate, Amyotrophic lateral sclerosis, Astrocytes, Microglia, Reactive oxygen species

ALS'in ön semptomatik aşamasında merkezi sinir sistemi sınırlı makrofajlarının (CNS-BAM'lerin) azaltılmasının nöroinflamasyon, semptomlar ve sağkalım üzerindeki etkisi

Narges SHOMALIZADEH

sinirbilim Ph.D., Şubat 2023

ÖZETÇE

Giriş: Amyotrofik lateral skleroz (ALS), ilerleyici kas atrofisi ile karakterize edilen tedavisi mümkün olmayan bir motor nöron hastalığıdır, bu atrofi solunum kaslarını da içerir. Kas zayıflığı, erime, kramplar ve fasikülasyonlar alt motor nöron kaybından kaynaklanır. Ayrıca, ALS'li hastalar frontotemporal kortekste nöron kaybı nedeniyle ekstra-motor belirtiler yaşayabilirler. Genellikle, hastalık başlangıcından sonra 2 ila 4 yıl arasında bir sürede solunum yetmezliği ölümün başlıca nedenidir. Yetişkinlerde en yaygın motor nöron hastalığı olan ALS'nin insidensi 100.000 başına 2 ve prevalansı 100.000 başına 5,4'tür. ALS patogenezine yönelik geniş kapsamlı çalışmalara rağmen, nörodejenerasyonun tam mekanizması net değildir.

Perivasküler makrofajlar (PVM'ler), santral sinir sisteminde (CNS) bulunan miyeloid hücrelerdir ve CNS sınırı ile ilişkili makrofajlar olarak bilinen daha büyük bir makrofaj grubunun bir parçasıdır. Sağlıklı bir durumda, bu hücreler damardan sızan zararlı maddeleri fagosite eder ve bağışıklık yanıtlarını düzenler. Ancak, iltihaplı bir durumda, artmış vasküler geçirgenliğe ve sonrasında nöroinflamasyona katkıda bulunurlar. Kan-beyin bariyerinin (BBB) disfonksiyonu ALS'nin semptomatik aşamasından önce meydana gelir ve PVM'leri etkiler, bu da reaktif oksijen türleri (ROS) üretiminde ve BBB geçirgenliğinde artışa neden olur. Dönüşmüş PVM'ler, diğer beyin miyeloid hücreleri ile iş birliği yaparak proinflamatuar süreçleri başlatır.

Amaç: Amacımız, PVM'lerin ALS patogenezine katkısını ve nöroinflamasyondaki etkilerini araştırmaktır. Bunun için, ALS'nin ön belirtili aşamasında PVM'leri azalttık ve bir hayvan modelinde mikroglia aktivasyonunu, astrogliyozu, BBB bozulmasını, semptomları ve yaşam süresini değerlendirdik.

Yöntem: PVM azaltımı, ALS hayvan modeli olan SOD1$^{(G93A)}$ mutasyonlu sıçanların serebrospinal sıvısına klodronat yüklü lipozomlar veya PBS yüklü lipozomlar (bir kontrol olarak) enjekte edilerek sağlandı. Çalışma, 59 SOD1 mutasyonlu sıçanı (hem erkek hem de dişi) içeriyordu. Ön çalışmalar dokuz sıçanı kapsarken, kalan elli sıçana klodronat yüklü lipozomlar (azaltılmış grup) veya PBS yüklü lipozomlar (yalancı işlem grubu) serebral enjeksiyon yoluyla verildi. Süspansiyondaki klodronat konsantrasyonu 5 mg/ml idi. Sıçanlar üç deneye ayrıldı: erken tek enjeksiyon, geç tek enjeksiyon ve doğumdan sonra 80. günde, doğumdan sonra 160. günde ve doğumdan sonra 80. günde ardışık 20 günde bir iki ek enjeksiyon yapılan çoklu enjeksiyonlar. Sıçanlar, insan son noktasına ulaşana kadar izlendi, ağırlık haftada iki kez ölçüldü ve nöromüsküler kuvveti, motor koordinasyonu ve dengeyi değerlendirmek için haftalık olarak lokomotor aktivite testi yapıldı. Lokomotor aktivite testi, yürüme analizi, kuyruk kaldırma, denge tahtası testi, pençe kavrama dayanıklılığı, uzatma refleksi, dikme davranışı ve yürürken pençe yerleştirme doğruluğu için merdiven basamağı testini içeriyordu.

Doğrulama çalışmaları, PVM'lerin SOD1 ve WT sıçanları arasında karşılaştırılması, enjeksiyon noktası doğrulaması ve PVM azaltımının doğrulanması için Sprague Dawley soyundan WT sıçanları içeriyordu. FITC-Albümin enjeksiyonu, beyne ve omuriliğe uygun teslimatı onaylayarak, sonraki çalışmalar için enjeksiyon noktasını doğruladı.

sıçan modellerinden elde edilen doku örneklerinde astroglia, mikroglia ve CD206+ hücreler için immunofluoresan boyama, sırasıyla GFAP, Iba 1 ve CD206 primer antikorları kullanılarak gerçekleştirildi. İstatistiksel yöntemler, üç denemede azaltılmış ve yalancı işlem grupları arasındaki davranış skorlaması ve ağırlık değişikliğini analiz etmek için kullanıldı.

Bulgular: SOD1 ve WT sıçanlarının CNS dokularında yapılan ön çalışmalar, SOD1 mutasyonlu sıçanların çeşitli beyin ve omurilik bölgelerinde CD206^{+} hücrelerin yukarı regülasyonunu gösterdi.

FITC-Albümin enjeksiyonu, beyin ve omuriliğe uygun teslimatı onaylayarak, PVM'lerle kollokale olan enjeksiyon noktasını sonraki çalışmalar için doğruladı.

WT sıçanların beyin ve omurilik kesitleri için CD206 ile immunofluoresan boyama, azaltılmış grupların tüm bölgelerinde CD206^{+} hücrelerin aşağı regülasyonunu gösterdi, özellikle çoklu enjeksiyon deneyi için omurilikte anlamlı sonuçlar elde edildi.

Ağırlık değişikliği analizi, üç denemede azaltılmış gruplarda gecikmiş ön belirtili aşamayı gösterdi, çoklu enjeksiyon deneyi için anlamlı sonuçlar elde edildi. Davranışsal çalışmalar, azaltılmış gruplarda daha hafif veya gecikmiş semptomatik aşamaları, özellikle çoklu enjeksiyon deneyinde doğruladı.

PVM'lerin, astrositlerin ve mikroglialarının immunofluoresan boyama ile ventral boynuzdaki tüm üç hücre tipinin upregülasyonunu, geç tek enjeksiyon ve çoklu enjeksiyon deneylerindeki azaltılmış gruba karşı yalancı işlem grubuna göre ortaya çıkardı.

Sonuç: Bu çalışma, ALS'nin ön belirtili aşamasında perivasküler makrofajların tükenmesinin hastalık başlangıcını geciktirebileceğini, özellikle klodronat yüklü lipozomların tekrarlayan dozlarını alan hayvanlarda gösterdi. Locomotor aktivite testleri ve ağırlık değişikliği kayıtları, bu hayvanlarda gecikmiş ve daha hafif semptomatik aşama gösterdi. Azaltılmış gruptaki ventral boynuzdaki $CD206^{+}$ hücrelerin, mikroglia ve astrositlerin upregülasyonu, bu gruptaki motor davranışların iyileştirilmesi ile ilişkili olan $CD206^{+}$ hücrelerin, astrositlerin ve mikroglialarının anti-inflamatuar fenotipi ile ilişkili görünmektedir.

Anahtar kelimeler: Perivasküler makrofajlar, Klodronat, Amiyotrofik lateral skleroz, Astrositler, Mikroglia, Reaktif oksijen türleri

ACKNOWLEDGMENTS

I am sincerely thankful to Professor Dr. Yasemin Gürsoy Özdemir for her invaluable guidance, steadfast support, and the trust she placed in me by granting the freedom to conduct the experiment. Our friendly relationship, coupled with her expertise and encouragement, has been crucial in shaping my research journey. I am truly grateful for the opportunity she gave me to work alongside her and for her exceptional mentorship. Also, I would like to thank Assoc. Prof. Dr. Atay Vural, Dr. Sebastian A. Lewandowski for their scientific guidance and kind support.

I would like to express my deepest gratitude to my lab mates, YGÖ team, whose support and collaboration have been invaluable throughout this journey. Special thanks to Dr. Esra Özkan for her dedication and insightful contributions, which greatly enriched our research endeavors. I am also grateful to Judy Kesibi, the purest soul, and Selcuk Polat, the resilient co-worker, for their constant encouragement and assistance, which played a pivotal role in the success of this project. Furthermore, I extend my appreciation to Feride Demirhan, Fatmanur Akpunar, Selin Selvi, Ceyda Özler, Alara su Bilgez, and Mahmud Mahmudi for their valuable companionship. Their collective efforts have significantly enhanced the quality of our work, and I am truly fortunate to have had the opportunity to collaborate with such talented individuals.

I am deeply grateful to my family, whose support has been the foundation of my journey. My beloved husband, Mohammad Amin Dadgar, has been a constant source of encouragement, understanding, and love, serving as my pillar of strength during the most challenging times. His consistent belief in me has propelled me forward, shaping my path to success. I am also grateful for the love, guidance, and sacrifices of my dear mother, Parvin Mehrnia. Her presence has played an integral role in shaping the person I am today. I am forever grateful for the support and encouragement of my late father, Mohammad Reza Shomalizadeh. His guidance has been my guiding light, illuminating my way through life's journey.

Special thanks to Joumana Alakhdar for her constant encouragement, understanding, and companionship. Her presence has brought **hope**, warmth and positivity to every moment shared.

I am also grateful to all my other friends who have stood by me with consistent support, offering their guidance, laughter, and endless encouragement. Deniz, Sahra, Hadi, Morteza, Farinaz, Shaghayegh, and Nazan Your friendship has enriched my life in countless ways, and I am deeply appreciative of each and every one of you. Together, you have made this journey more meaningful and memorable, and I am truly blessed to have such amazing friends in my life.

Table of Contents

TABLE OF CONTENTS

List of tables

List of figures

List of figures

Chapter 1

1 Introduction

Amyotrophic lateral sclerosis (ALS) is an incurable motor neuron disease that affects both upper and lower motor neurons, leading to progressive muscle atrophy, including respiratory muscles. Lower motor neuron loss extending from the spinal cord results in muscle weakness, wasting, cramps, and fasciculations. ALS also involves extra-motor systems to varying degrees, with some patients experiencing cognitive and behavioral symptoms due to frontotemporal cortex neuronal loss (Oskarsson et al.). The typical survival period after disease onset is 2-4 years, with respiratory failure being the primary cause of death. With an incidence of 2 cases per 100,000 individuals and a prevalence of 5.4 cases per 100,000, ALS stands as the most common adult motor neuron disease (Chiò et al., 2013).

Approximately 10% of ALS cases are familial, with several identified genetic factors associated with familial ALS, such as C9orf72 repeat expansion, mutations in genes encoding SOD1, FUS, TDP-43, and about 30 other genes. Mutations in TARDBP, the gene encoding the TDP-43 protein, are a primary contributor to protein aggregation in cells. These protein aggregates induce neuronal dysfunction and cell death in most ALS patients, irrespective of familial or sporadic cases. Although the exact mechanism of neurodegeneration induction is unclear, it is believed that these inclusions may be toxic themselves or hinder the protein's normal function in cells (Oskarsson et al.). In addition to issues related to protein translation and degradation, various pathological mechanisms play a role in different stages of the ALS neurodegenerative process. These include mitochondrial dysfunction, oxidative damage, glutamate excitotoxicity, inflammation, and dysregulation in intracellular and nucleocytoplasmic transport (Rothstein, 2009).

1.1 Epidemiology

1.1.1 Risk factors

Various non-genetic factors contribute to an elevated risk of developing ALS. Lifestyle choices, environmental and occupational factors, pre-existing medical conditions, comorbidities, and medical exposures are all linked to the incidence of ALS.

In terms of lifestyle factors, research indicates that current smoking significantly heightens the risk of ALS, especially when compared to past smoking habits. Among non-genetic factors, environmental and occupational exposures hold particular significance. Exposure to pesticides, heavy metals, and solvents has been shown to notably increase the risk of ALS. While the impact of electromagnetic field exposure on ALS incidence remains unproven, the intensity of exposure may influence the development of ALS. Epidemiologically, heavy metals such as lead, mercury, and selenium are associated with an increased risk of ALS, potentially inducing neurodegeneration by disrupting TDP-43 homeostasis in neurons. Pre-existing conditions, including head trauma, stroke, and hypertension, are identified as risk factors for ALS. Studies examining the correlation between head trauma and ALS risk reveal a clear association, with a history of head trauma linked to ALS development. Animal models involving rats and drosophila demonstrate that brain trauma can cause defects in nucleocytoplasmic transport, potentially initiating TDP-43 pathology in neurodegenerative diseases. Conversely, diabetes exhibits a modest protective effect, aligning with earlier research indicating a link between diabetes and delayed ALS onset. This supports the notion that disturbances in metabolism may play a role in the clinical progression of ALS. Additionally, the use of antidiabetic medications emerges as a significant factor in ALS prevention, possibly influenced by the administration of oral hypoglycemic drugs to diabetic individuals. Notably, kidney disease, akin to diabetes, demonstrates a protective influence on the occurrence of ALS.

Moreover, regarding non-genetic factors, research provides substantial evidence regarding the impact of military service on the occurrence of ALS. Additionally, studies confirm that a high body mass index (BMI) acts as a protective factor against the onset of ALS. Subgroup analysis further underscores that obesity exerts a more pronounced

protective effect on ALS in comparison to being overweight, highlighting the correlation between weight loss and shorter survival in individuals with ALS.

Although genetic factors play a limited role in ALS onset, they offer crucial insights into the underlying mechanisms of the disease. Pooled analysis has identified seven candidate ALS causative genes, contributing to approximately 10% of ALS cases across all patients. Mutation frequencies were notably higher in European patients and those with familial ALS (FALS), underscoring the relevance of genetic factors. The overall pooled mutation frequencies for major ALS-related genes were 2.2% for SOD1, 2.1% for C9orf72, 1.7% for ATXN2, 1.7% for FUS, 0.8% for TARDBP, 0.6% for VCP, 0.6% for SQSTM1, and 0.6% for UBQLN2. Subgroup analysis based on family history revealed mutation frequencies of 28.6% in FALS and 8.1% in sporadic ALS (SALS), indicating a higher gene mutation rate in familial cases and underscoring the importance of genetic testing in FALS. The top three mutated genes in FALS were SOD1, C9orf72, and FUS, while in SALS, they were ATXN2, SOD1, and FUS. The distinct genetic structures between FALS and SALS emphasize the need for careful consideration during genetic testing in ALS patients. Subgroup analysis also revealed differences in gene mutation patterns between European and Asian populations. In European populations, C9orf72 repeats were the most common mutations in ALS, followed by SOD1, ATXN2 repeats, FUS, TARDBP, VCP, UBQLN2, and SQSTM1. In Asian populations, SOD1 mutations were the most prevalent, followed by C9orf72 repeats, FUS, ATXN2 repeats, SQSTM1, TARDBP, UBQLN2, and VCP. These findings suggest a higher frequency of gene mutations in European populations, with significant variations in mutant spectra among different populations (Duan et al., 2023).

1.2 Cellular and molecular pathways contributing to ALS

It has been hypothesized that the selective motor neurons degeneration in ALS may be attributed to the involvement of neighboring astrocytes rather than occurring through a cell-autonomous process (Rothstein, 2009). Numerous studies verify the involvement of astrocytes, and deficiencies in their glutamate transporter have been identified in a significant proportion of sporadic ALS patients as well as in rodent models with SOD1 mutations. (Howland et al.; Rothstein et al.). It has been demonstrated that astrocytic inclusions precede the onset of symptoms in a model of SOD1 mutant toxicity. These inclusions develop rapidly with the progression of the disease and are associated with a

decrease in the glial glutamate transporter (GLT-1). Based on these findings, it is concluded that SOD1 mutations inflict damage on astrocytes, potentially contributing to the degeneration of motor neurons (Bruijn et al.). Astrogliosis refers to the remodeling of astrocyte biology in response to central nervous system (CNS) damage, which includes neurodegeneration. The characteristics of reactive astrocytes vary depending on their proximity to the damage and the nature and severity of the insult. Severe astrogliosis results in the proliferation of astrocytes and the formation of glial scars, while milder forms do not exhibit these features. Astrogliosis is a complex, multicellular phenomenon involving not only astrocytes but also other non-neuronal cells such as microglia, oligodendrocytes, and endothelial cells, as well as neuronal cells (Pehar et al.). Glial cell's key role in motor neuron fate and disease progression has been confirmed by several studies (Beers et al.; Di Giorgio et al., 2007; Ferraiuolo et al.; Nagai et al.). The selective elimination of the $SOD1^{G93A}$ transgene from glial cells in $SOD1^{G93A}$ mice or the replacement of wild-type astrocytes or microglia in the central nervous system (CNS) of these animals has been shown to decrease the speed of disease progression and extend lifespan (Boillée et al.; Clement et al.; Wang et al.; Yamanaka et al.). These studies have shed light on the involvement of toxic features of mutant SOD1 transgene in glial cells in the emergence of ALS. Consequently, therapeutic approaches aimed at reducing SOD1 have been developed in alignment with the findings from these experiments (McCampbell et al.).

Neurotoxic reactive microglia, referred to as the M1 phenotype, becomes activated in response to neuroinflammatory insults. The transformation of astrocytes from a quiescent state to a reactive phenotype, known as A1, is initiated by M1 microglia through the secretion of inflammatory cytokines such as IL-1α, TNFα, and C1q. Studies involving mice lacking microglia have revealed that these animals were unable to induce A1 astrocytes in response to lipopolysaccharide (LPS) injection. This led to the conclusion that microglia is a crucial factor in facilitating the acquisition of toxic functions by astrocytes (Liddelow et al., 2017). The significant extension of lifespan in the ALS mouse model was observed upon the elimination of IL-1α, TNFα, and C1q, emphasize the crucial role of these factors in the progression of ALS. The impact of A1 astrocytes on ALS pathogenesis has been assessed through the examination of C3 and GFAP staining on tissue sections obtained from both familial and sporadic ALS patients. Additionally, the measurement of C3 mRNA expression in the spinal cord of ALS patients has been

employed to further elucidate the role of A1 astrocytes in the progression of ALS (Guttenplan et al., 2020).

As mentioned previously, A1 astrocytes undergo a transformation, acquiring new biological features. These A1 astrocytes exert a toxic effect by secreting one or more harmful factors specifically targeting neurons and oligodendrocytes. Interestingly, their toxic influence is not directed towards endothelial cells or pericytes (Di Giorgio et al., 2007; Liddelow et al., 2017; Nagai et al.). In general, it appears that the microglia-to-astrocytes axis plays a promotive role in disease progression in ALS rodent models. Notably, microglia alone seem to be insufficient to induce neuronal death (Guttenplan et al., 2020; Liddelow et al., 2017). The mechanism by which reactive astrocytes promote the death of neurons and oligodendrocytes involves the delivery of free fatty acids (FFAs) and very-long-chain fatty acid acyl chains (VLCPCs). This process is likely facilitated through the secretion of lipoparticles (Guttenplan et al., 2021). The role of lipids in central nervous system (CNS) signaling by astrocytes and microglia remains insufficiently studied. The trafficking of lipids in reactive astrocytes expressing various APOE isoforms is unclear. Despite the recognized involvement of saturated lipids in neuroinflammation and neurotoxicity, reducing these lipids from reactive astrocytes' conditioned medium does not eliminate neurotoxicity in vitro. This incomplete efficacy may stem from potential challenges in completely knocking out the lipids or the influence of toxic proteins, microRNAs, or other lipids present in the conditioned medium (Guttenplan et al., 2021).

Reactive oxygen species (ROS) are oxygen-containing molecules, both radical and nonradical, that result from the incomplete reduction of oxygen. Examples include the superoxide radical anion (O2•-), hydrogen peroxide (H2O2), and the hydroxyl radical (HO•). These species are produced as by-products of cellular metabolism through enzymatic and nonenzymatic reactions. The generation of ROS is a natural part of cellular processes, but excessive or uncontrolled production can lead to oxidative stress, causing damage to cellular components and contributing to various pathological conditions. In addition to various mechanisms that produce ROS inside of the mitochondria, there are enzymes outside of it that are involved in ROS production such as nicotinamide adenine dinucleotide phosphate oxidase (NOX), xanthine oxidase, cyclooxygenases, CYP450, and lipoxygenases (Pizzino et al., 2017).

Enzymatic and nonenzymatic antioxidants contribute to cellular defense against oxidative stress. Several key enzymes are active in reducing reactive ROS, including superoxide dismutases, catalase (CAT), glutathione peroxidase (GPx), glutathione reductase (GR), and thioredoxin (Trx). This defense system is supplemented by nonenzymatic antioxidants, including glutathione (GSH), vitamins A, C, and E, flavonoids, and proteins such as albumin, ceruloplasmin, and metallothionein. There is an imbalance between heightened ROS production and ineffective antioxidant defenses in ALS. The dysregulation of ROS and antioxidant mechanisms contributes to oxidative stress, which contributes to the progression of ALS (Cunha-Oliveira et al., 2020).

1.2.1 Neurovascular Unit Dynamics

The blood-brain barrier (BBB) serves as a specialized structure, regulating the exchange of substances between the blood and the brain parenchyma, crucial for brain metabolism and waste removal. Disruption of the BBB and cerebrovascular malfunction are identified as detrimental factors that can initiate various CNS disorders. It is suggested that neuroinflammation resulting from cerebrovascular dysfunction may underlie the development of CNS disorders. Recent findings indicate that the upregulation of perivascular fibroblasts (PVFs) and subsequent remodeling of the perivascular space, marked by its enlargement, precede the symptomatic stage of ALS in both humans and $SOD1^{G93A}$ mice. Particularly, these changes occur earlier than the upregulation of microglia and astrocytes (Månberg et al., 2021). This fact indicates that alterations in the neurovascular unit precede the activation of microglia and astrogliosis. In other words, the initiation of neuroinflammation can be traced back to the disruption of the BBB. While there has been extensive research on the components of the neurovascular unit and the role of glial cells in neuroinflammation in recent decades, the precise timing and mechanisms underlying the impact of vascular components on parenchymal components, or vice versa, remain incompletely understood. In addition to microglia, several myeloid populations have been identified, demonstrating their essential role in sustaining brain homeostasis, and contributing to brain disorders. Non-parenchymal or CNS border associated macrophages (BAMs) are notable among these, comprising perivascular, subdural meningeal, and choroid plexus macrophages. In embryonic development, these macrophages are derived from yolk sac precursors. Except choroid plexus macrophages, these populations are not replenished by blood monocytes during adulthood (Siret et al., 2022). BAM's role in the progression of ALS is not well-studied.

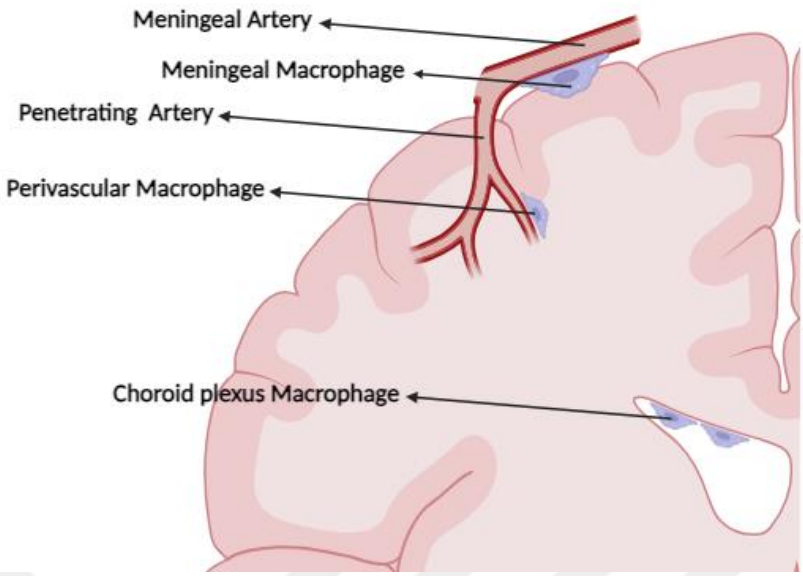

Figure 1-1 Brain associated macrophages (BAMs) including meningeal macrophages, perivascular macrophages, and choroid plexus macrophages (figure is created by Biorender.com)

Perivascular macrophages constitute a distinct group of immune cells associated with cerebral vessels. Recent advancements in microscopy and immunohistochemistry have enabled the differentiation of PVMs from microglia. Positioned on the abluminal side of cerebral blood vessels, PVMs express the mannose receptor CD206 in addition to CD11b, a marker expressed by all myeloid cells (Goldmann et al., 2016). Additionally, perivascular macrophages express the lymphatic vessel endothelial hyaluronan receptor-1 (LYVE1) and demonstrate lower levels of Iba-1 compared to microglia. Notably, these cells are actively involved in phagocytic activity (Bechmann et al., 2001; Zeisel et al., 2015). It is crucial to avoid confusion between PVMs and parenchymal microglia located adjacent to cerebral vessels. Typically, microglia and PVMs can be distinguished using the $CD45^{lo}CD11b^{+}CD206^{-}$ and $CD45^{hi}CD11b^{+}CD206^{+}$ marker combinations, respectively (Goldmann et al., 2016). The research indicates that PVMs are situated within the perivascular space of arterioles and venules. This space exists between the abluminal surface of the endothelial vessel basement membrane and the parenchymal basement membrane on the glia-limitans side. Importantly, PVMs are not found in association with capillaries, as there is no perivascular space around capillaries due to the fusion of these two membranes (Iadecola; Koizumi et al., 2019). PVMs exhibit the ability

of self-proliferation, which contributes to their longevity and preservation throughout the organism's life. Their sustained presence is a result of this intrinsic property, rather than being reliant on the infiltration of peripheral myeloid cells (Goldmann et al., 2016).

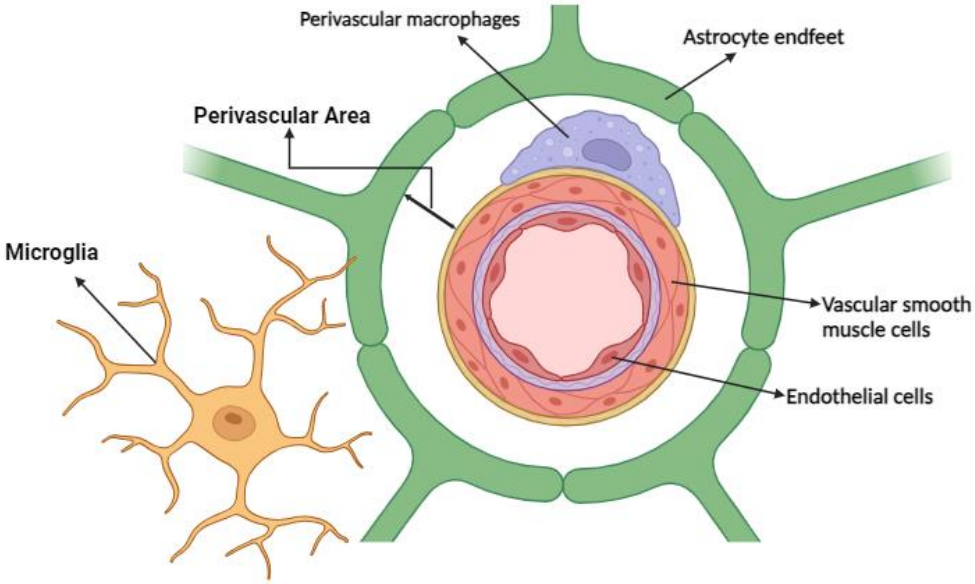

Figure 1-2 Perivascular macrophages position in the neurovascular unit (figure is created by Biorender.com)

1.3 Background studies on PVMs

In several studies examining the impact of PVMs on cerebrovascular dysfunction in CNS diseases, evidence suggests their role in increasing vascular permeability. Notably, in a transient middle cerebral artery occlusion (tMCAO) model during the acute phase of stroke, it was observed that PVMs contribute to heightened vascular permeability concurrent with granulocyte recruitment. Interestingly, the depletion of PVMs using clodronate liposomes resulted in a reduction of both vascular permeability and granulocyte infiltration in the ischemic cortex (Pedragosa et al.).

In another study involving an acute hypertension model, it was demonstrated that the generation of ROS by PVMs via the Angiotensin II type 1 receptor (AT1R), coupled with the activation of Nox2 in PVMs, resulted in an increased BBB permeability. Depletion of PVMs using clodronate liposomes did not alter baseline cerebrovascular responses but

effectively restored the neurovascular dysfunction observed in a genetic model of lifelong hypertension and in the hypertension model induced by the gradual administration of angiotensin II (ANGII) (Faraco G Fau - Sugiyama et al.). Depletion of PVMs through clodronate liposome administration in a chronic hypertensive model prevented structural remodeling of the medial cerebral artery induced by hypertension. Additionally, this intervention led to an improvement in the endothelium-dependent dilation of the artery (Pires et al., 2014). The role of PVMs in cerebral amyloid angiopathy (CAA), characterized by the deposition of Aβ in cortical blood vessels, was examined in a mouse model of Alzheimer's disease (AD). Depleting PVMs with clodronate liposomes resulted in an increase in amyloid depositions within cortical vessels in the animal model. This suggests that PVMs play a critical role in Aβ clearance through phagocytosis. However, enhancing clearance capacity may be associated with an elevated production of ROS (Hawkes & McLaurin, 2009). In another study, it was demonstrated that the production of ROS and cerebrovascular dysfunction induced in various Alzheimer's disease models was reduced through intracerebroventricular injection of clodronate liposomes. Additionally, the study revealed that the CD36 and Nox2 receptors of PVMs contribute to the neurovascular dysfunction induced by amyloid deposition (Park et al.).

1.4 Aim of the project

In this study, our objective is to investigate the contribution of PVMs to ALS disease pathogenesis and their impact on neuroinflammation. We hypothesize that the dysregulation of the BBB, occurring well before the symptomatic stage of ALS, influences the characteristics of PVMs, potentially leading to an increased generation of reactive oxygen species. These alterations in PVMs could result in heightened BBB permeability. Collaborating with other brain myeloid cells, these transformed PVMs may initiate the neuroinflammation process. To test this hypothesis, we aim to deplete PVMs to assess whether the severity of microglia activation, astrogliosis, BBB disruption, symptoms, and the lifespan of the animal model are altered after repopulation of PVMs.

Chapter 2

2 Materials and methods

2.1 Experimental design

This study was applied in accordance with the required protocols and guidelines of the Koç University Institutional Animal Care and Use Committee (IACUC) based on the European Parliament and Council's Directive 2010/63/EU on the protection of animals used for scientific purposes. In addition, all experiments were conducted according to the guidelines for reporting animal research in vivo experiments (ARRIVE). The rats were housed in plastic cages and maintained at a controlled temperature (22°C/12-hour light/dark cycle) with free access to food and water.

2.1.1 Animal model

To model ALS, we used $SOD1^{G93A}$ transgenic rats. The wild-type (WT) and $SOD1^{G93A}$ rats (Sprague Dawley background) were housed in the animal facility at Koç University. Due to the dominance of the SOD1 gene, we used heterozygotes that have a longer life span. Our goal is to obtain heterozygote rats by mating SOD1-positive rats (determined by genotyping as discussed below) with WT rats.

2.1.2 Characterization of colony and PVMs in SOD1 rats

In order to characterize the colony, nine SOD1 rats were followed until they reached their human end point. Upon reaching the end point, each of them was terminated along with a WT rat from the same generation. Four SOD1 and corresponding four WT tissues were processed for this step.

2.1.3 hSOD1 ^{G93A}

We have discussed before that the $SOD1^{G93A}$ positive rats were mated with their WT litter mates in order to produce heterozygotic pubs. Three weeks after their birth, the pubs were separated from their mother for the purpose of taking a tail sample for DNA extraction and genotyping. The DNA is isolated using the Quick-DNA^{TM} Miniprep Plus

kit (ZYMO Research). A Nanodrop machine was used to measure the DNA concentration of the samples following DNA isolation.

Forward and reverse primer sequences for SOD1 are "GTG GCA TCA GCC CTA ATC CA" and "CAC CAG TGT GCG GCC AAT GA" respectively. In order to perform gradient PCR, we prepared a dilution of 10 M of the primers' main stock.

A volume containing 100 ng of the isolated DNA was set to 10 µl (by adding nucleus free water) then the following mixtures were added: 1.25 µl of forward primer, 1.25 µl of reverse primer, and 12.5 µl of PCR master mix (brand name). Each sample should have a total volume of 25 µl. The microtubes were then placed in the thermal cycler (T100™ Thermal Cycler, BIO-RAD) as follows: at 95 °C for 1 minute, 35 × (95 °C for 15 seconds, 62.1 °C for 15 seconds, and 72 °C for 20 seconds), 72 °C for 8 minutes, and 12 °C for infinity. The lid temperature is 105 °C.

The electrophoresis gel was made from 1% agarose in 1×TAE solution and 0.2% Ethidium bromide. After this, 10 µl of each sample (obtained from gradient PCR) were added to each well. The first well was also loaded with 6 µl of gene ruler to ensure that the bands opened in the correct position. An electrophoresis of 30 minutes at 100 volts was carried out.

To visualize the gel, it was transferred to an imaging system (ChemiDoc™ MP, BIO-RAD).

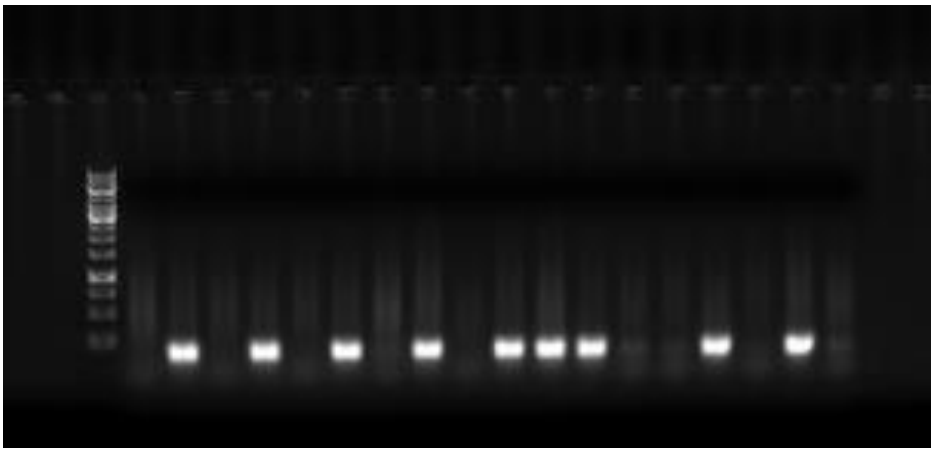

Figure 2-1 Example image taken from ChemiDoc™ imaging system. The bright bands show expression of the hSOD1 gen.

2.1.4 Chemicals

2.1.4.1 Drug

The purpose of depleting PVMs is to investigate whether they contribute to the deterioration of neurovascular function in ALS patients, specifically in the SOD1 transgenic model. For this purpose, we depleted PVMs using Liposomes loaded with clodronate (LIPOSOMA, Amsterdam). Macrophages phagocytose clodronate, which induces cell death via programmed cell death.

Liposomes are artificially synthesized spheres composed of concentric layers of phospholipids. Following dispersion in water, phospholipids form liposomes that have hydrophilic heads on their outer surfaces and hydrophobic fatty acid groups on their inner surfaces. Aqueous compartments separate these bilayers, allowing hydrophilic molecules to dissolve in them and encapsulate them within the liposome. As a hydrophilic molecule, Clodronate, also known as dichloroethylene-bisphosphonate or Cl_2MBP, can be encapsulated within these phospholipid bilayers.

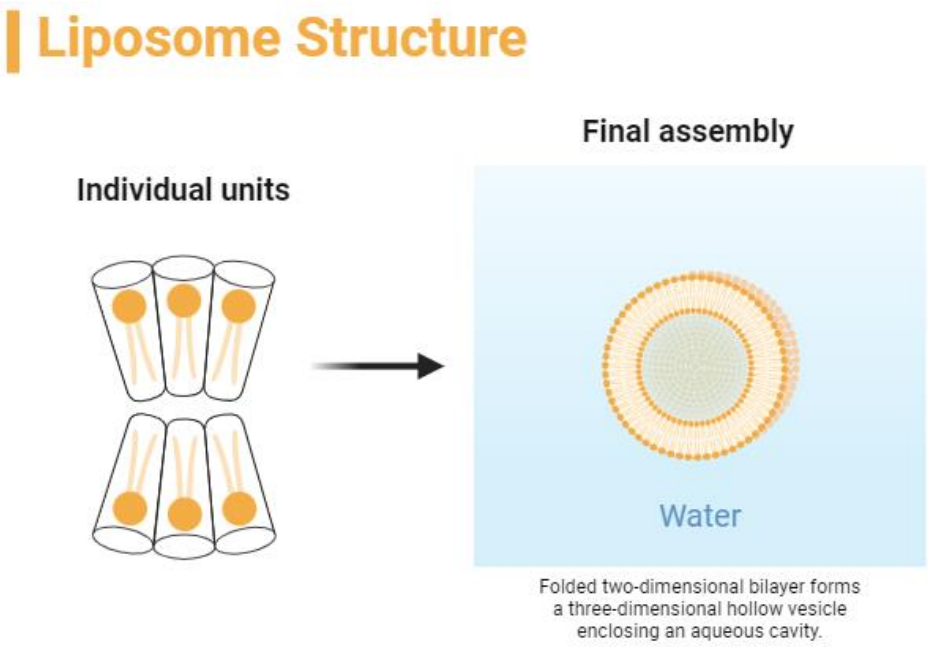

Figure 2-2 liposome structure. Amphiphilic phospholipid molecules form bilayer spheres upon dispersion in aqueous medium (created by Biorender.com).

Free clodronate encounters obstacles in crossing cell membranes and is rapidly eliminated from circulation by the renal system within minutes. However, when clodronate is entrapped in a liposome, it becomes engulfed by macrophages, preventing its escape. While lysosomal phospholipases digest the phospholipid bilayers, clodronate remains intact within the macrophage. As macrophages ingest more phospholipid bilayers and liposomes, the accumulation of clodronate within the macrophage increases. Once the intracellular concentration goes beyond a certain threshold, clodronate induces apoptosis, leading to the depletion of the macrophage.

Upon the injection of clodronate-loaded liposomes, the depletion of perivascular and meningeal macrophages initiates. The maximum impact is observed in the second week after injection, and by day 14 post-injection, brain border-associated macrophages begin to repopulate. Approximately thirty days after the injection, the cell population returns to its initial state (Polfliet et al., 2001).

2.1.4.2 injection method

Based on their injection age and number of injections, there are three general groups in the main experiment: early single injections (80 days after birth), late single injections (160 days after birth), and multiple injections (first injection at 80 days after birth, followed by two more injections every three weeks thereafter). Each group is divided into a sham group and a treatment group. The sham groups received PBS-loaded liposomes, while the treatment groups received clodronate-loaded liposomes. A total of 50 transgenic animals were used in this study. We injected 30 µl clodronate- or PBS-loaded liposomes suspension into the cisterna magna using a micro injector (Hamilton®, gauge 33, blunted). The animals were anesthetized by using lower dose of ketamine xylazine cocktail (30 mg/kg ketamine) kept sedated under 1-2% isoflurane while the animal was fixed in the stereotaxic frame. Injections were carried out at a rate of 2.5 µl per minute by using injector pump. In order to inject into the cisterna magna, the animal was placed in the stereotaxic frame with its nose pointed downwards. To expose the skin, the fur was shaved. In the next step, the skull's posterior end was located at the level of the ears, and the skin was cut along the midline. In the anterior-to-posterior axis, the cisterna magna can be exposed by pulling the neck muscles apart from the midline. A transparent dural membrane covers the cisterna magna, which has an inverted triangle shape and is located

between the cerebellum and the medulla at the base of the skull. By penetrating the syringe tip into the cisterna magna, clodronate- or PBS-loaded liposomes were injected.

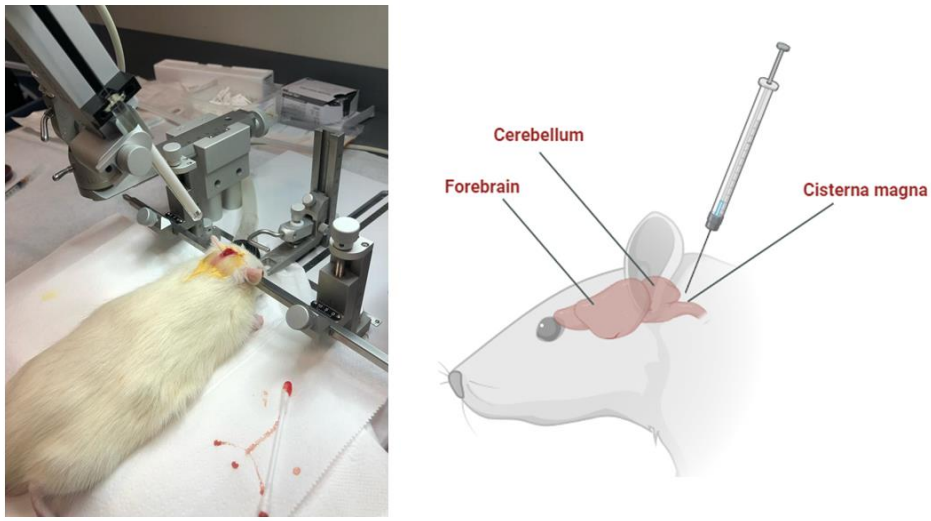

Figure 2-3 Rat placement in the stereotaxic device. The Clodronate or PBS-loaded liposome suspension is injected by using micro injector to cisterna magna. The injector pump was set on 2.5 µl per minute.

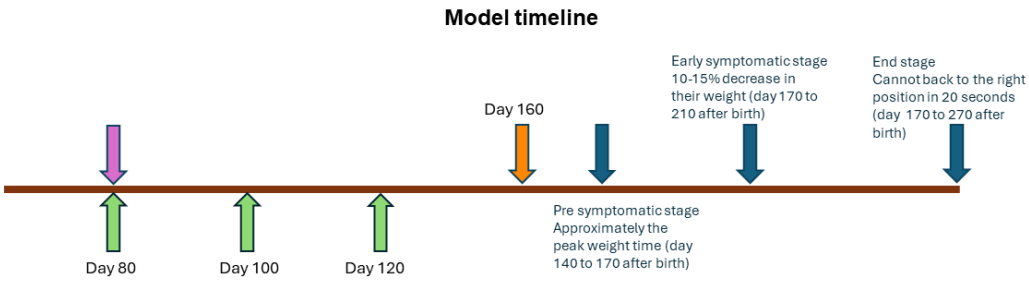

Figure 2-4 animal model timeline. Green arrows show the injection days of multiple injection experiment. Purple arrow indicates injection day for early single injection, and orange arrow the late single injection. Dark blue arrows specify the disease stages.

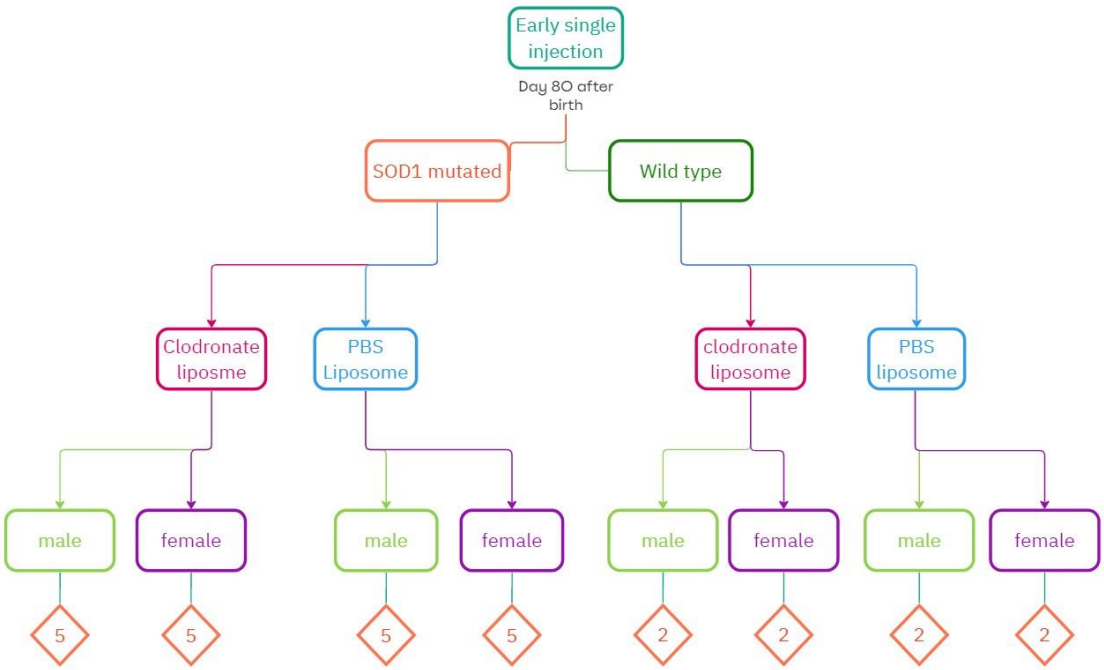

Figure 2-5 Groups, animal numbers and their gender in early single injection experiment.

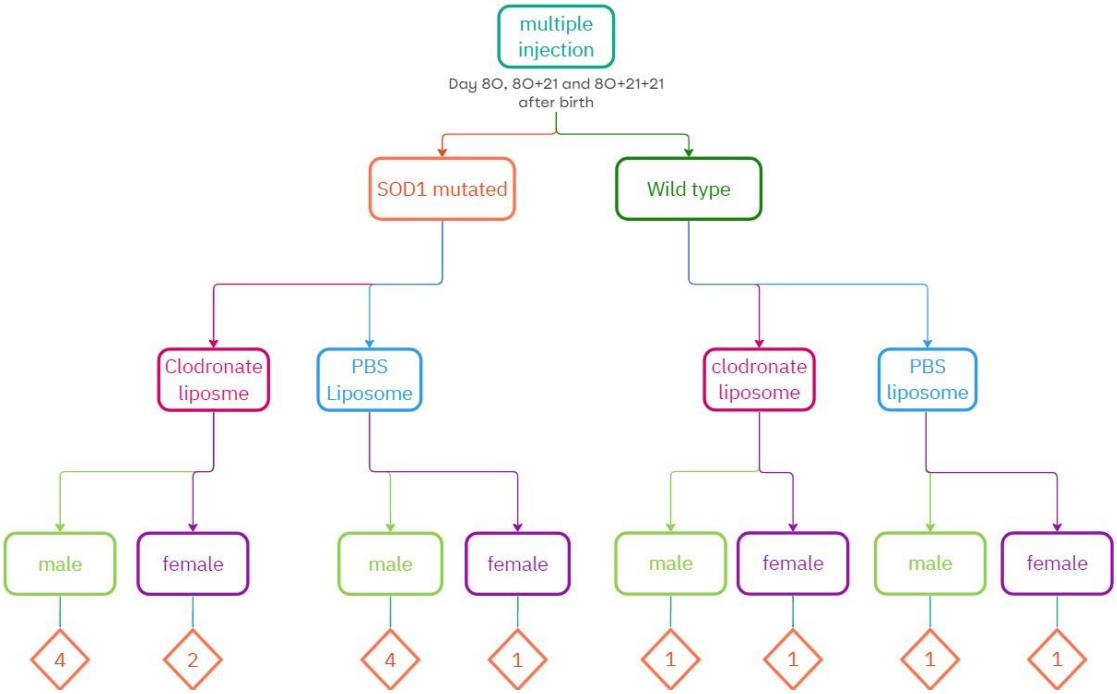

Figure 2-6 Groups, animal numbers and their gender distribution in multiple injection experiment.

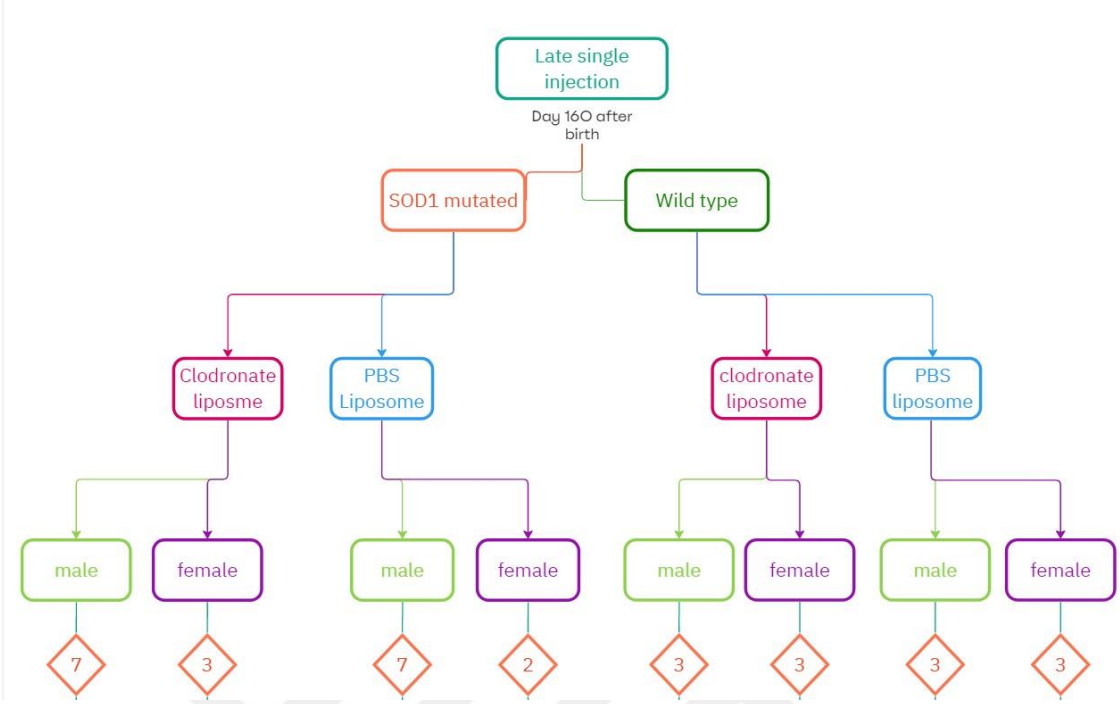

Figure 2-7 Groups, animal number and gender distribution in late single injection experiment.

2.1.4.3 Injection point validation

The injection point must be validated before we begin the experiment with the ALS rat models. In order to accomplish this, two wild type rats of the Sprague Dawley strain were anesthetized (75mg/kg ketamine xylazine cocktail) and then FITC albumin was injected into their cisterna magna according to the method explained before. One hour later, the rats were perfused with PBS and then 4% PFA. Following decapitation, the brain and spinal cord were dissected for further analysis. The tissues were treated to be ready for immunofluorescence staining (the method is described later). Tissue sections were stained with CD206 primary antibody and mounted with Dapi. Using fluorescent microscopy, the diffusion of FITC albumin from the cisterna magna to various locations in the brain and spinal cord is examined.

2.1.4.4 Validation of PVMs depletion after clodronate liposome injection

During this step, we validated the depletion of PVMs after clodronate-loaded liposomes were injected into the cisterna magna. We recruited another group of 10 wild

type animals. Half of them received clodronate-loaded liposomes, and the other half received PBS-loaded liposomes. The age of the rats receiving either PBS or clodronate-loaded liposomes was the same as that of the main experiment group. There are three groups, one early injection, one late injection, and multiple injections, similar to the main experimental groups. After two weeks of injection (last injection for those receiving multiple injections), the animals were perfused with PBS followed by 4% PFA. Dissected tissues were prepared for immunofluorescence staining in the same manner that will be described later. We used the CD206 primary antibody as a marker for PVMs and the IB4 primary antibody as a marker for vessels.

2.1.5 Behavioral tests

The weight measurement and locomotor activity scoring were performed until the human endpoint, at which time the animals were sacrificed. We evaluated the animals' neuromuscular strength, motor coordination, balance, and so on through behavioral tests.

A series of six assessments is used to determine the onset and progression of the disease (Haulcomb et al.). The test was conducted once a week at the same time on each testing day, approximately six hours into the light cycle. Every testing day, the order of the tests was changed. Testing was conducted by the same handler, who was blind to the groups, and the sessions were recorded. Open field boxes with transparent walls measuring 100 x 100 x 50 cm were used for three of the tests. The tests and their scoring systems are listed as following:

2.1.5.1 the rats were observed for 4 minutes in the open field:

2.1.5.1.1 Gait analysis test:

6	normal posture, gait, and forward motion
5	abnormal posture or trunk position during forward motion, such as a hunched appearance or sloped rump
4	waddling or lateral wobbling movement of the pelvis during forward motion
3	dysmetria or incoordinate movements with a distinct jerky, oscillating component during forward motion
2	at least one knee contacts ground during forward motion;
1	inability to properly place at least one hind foot flat during forward motion, often manifests as knuckle walking
0	at least one hindlimb is paralyzed, inability to move the hindlimb results in dragging limb during forward movement.

Table 2-1 Scoring description for gait analysis.

2.1.5.1.2 Rearing behavior:

5	rearing behaviour with complete extension/stretching of the hind-limbs at least twice
4	rearing behaviour was not performed or performed only once. Regardless of the extension situation
0	rearing behaviour with partial/incomplete extension/stretching of the hind limbs was observed at least twice

Table 2-2 scoring description for rearing behavior test.

2.1.5.1.3 Tail elevation:

5	Tail elevation level is higher that or at the level of the body during forward movement
3	Tail appears to slump during forward movement, distal portion of tail is lower that the body and routinely touches the ground
0	Tail is not elevated during forward movement, the entire tail or the distal portion drags on the ground

Table 2-3 scoring description for tail elevation monitoring.

2.1.5.1.4 Paw-grip endurance (by placing animal on a mesh and turning the mesh to vertical position):

5	grasp with all paws for 5 seconds
4	temporarily grasp with all paws for less than 5 seconds and suspected to release intentionally
3	temporarily grasp with all paws for less than 5 seconds and unintentionally release
1	grasp with forepaws only for less than 5 seconds
0	unable to maintain grip with paws

Table 2-4 scoring for paw-grip endurance test.

2.1.5.1.5 Extension reflex (5 seconds suspension by tail):

7	complete fore-and hind-limb extension
6	complete fore- limb extension and partial hind-limb extension
5	partial fore- and hind-limb extension
2	partial forelimb but no hind-limb extension
0	no fore- or hind-limb extension

Table 2-5 Scoring description for testing extension reflex.

2.1.5.1.6 Balance beam test (suspend the animal by tail and keep it near the beam under it if it grasps the beam then release the tail if not put the rat on the beam and wait for 5 seconds):

5	lift to beam with 4 paws, and don't fall within 5 seconds
4	lift to beam with only fore-paws, and doesn't fall within 5 seconds
3	lift to beam with only fore-paws, and fall within 5 seconds
1	unable to lift body onto the beam, after placed onto the beam by handler can stay for 5 seconds
0	unable to lift body onto the beam, after placed onto the beam by handler cannot stay for 5 seconds

Table 2-6 scoring description for balance beam test monitoring.

2.1.5.2 Ladder rung walking test:

Rats in this test walk from a neutral cage to a familiar cage on a pathway. This pathway consists of two Plexiglas panels with dimensions of 100 x 20 cm. The transparent walls are connected by removable rungs that provide a floor for the walking test. Rungs consist of wooden sticks with a diameter of 3 mm. In order to make the test unpredictable for the rats, the pattern of the rungs can vary. The apparatus should not be wider than the animal by more than one centimeter.

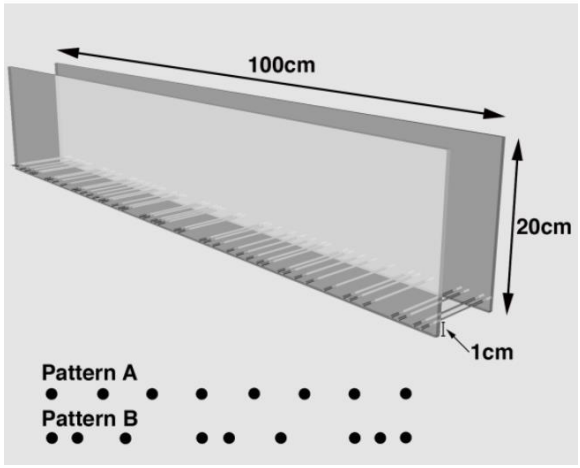

Figure 2-8 frontotemporal view of the ladder rung walking test apparatus, and two example for the rungs placement, regular and irregular (Metz & Whishaw).

It is possible to vary the distance between two rungs between 1 and 5 cm. During the test, the front and end edges of the apparatus are placed on the cages at a distance of 30 cm from the floor. However, for training purposes, two cages are placed on top of each other, resulting in a distance of 60 cm.

Each animal is subjected to three trials per testing day. Steps and errors (limbs falling between rungs) are counted separately for each pass. The mean number of errors per step and the average of all three trials are calculated (Metz & Whishaw).

2.1.6 Sacrifice and tissue collection

During the experiment, we anesthetized the animals with ketamine xylazine cocktail, transcardially perfused them with ice-cold DPBS followed by 4% PFA, and immersed their brains and spinal cords overnight in 4% PFA at a temperature of +4°C. Then, the tissues are processed as below for later experiments.

2.1.7 Immunofluorescence Staining and imaging

To demonstrate the relationship between PVMs and the vessels, along with the other components of the NVU, immunofluorescence staining was employed. We dehydrated the collected brains and spinal cords using a gradient of sucrose in dH2O at +4 °C (10%, 20%, and 30% incubated overnight in each dilution). Following this, we cut the brain and spinal cord into four parts as shown in the schematic below and embed and freeze them in OCT gel (DDK, Italy).

Later, we sliced them at a thickness of 20 µm and collected the sections on positive charged Superfrost™ Plus microscopy slides (Epredia, Netherlands). Then, we did the IF staining according to the following protocol:

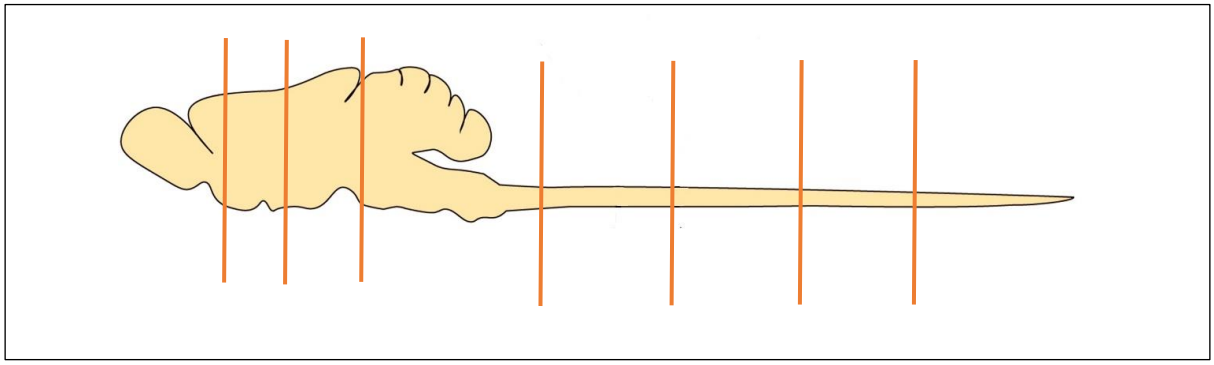

Figure 2-9 Schematic rat CNS. The lines show the cut positions.

2.1.7.1 IF protocol

1. Immerse the slides in dH2O for 5 minutes at room temperature.

2. Submerge the slides in PBS three times for 5 minutes each at room temperature.

3. Permeabilize by dipping in 0.5% Triton X100 in PBS at room temperature.

4. Rinse with PBS.

5. Outline the tissues with a hydrophobic marker (Peppen, brand).

6. Incubate in Superblock (brand) for 1 hour at room temperature.

7. Remove the Superblock.

8. Incubate in the primary antibody, CD206 (catalog number), at a 1:200 dilution in Superblock, at +4 °C overnight.

9. Wash the slides with 0.025% Triton X100 in PBS, 4 times for 5 minutes each on a shaker (30 rpm).

10. Remove excess liquid around the tissues and incubate in the secondary antibody, Cy3 (brand and catalogue number), at a 1:200 dilution in Superblock, at 37 °C for 90 minutes.

11. Wash the slides with 0.025% Triton X100 in PBS, 4 times for 5 minutes each on a shaker (30 rpm).

12. Repeat steps 8 to 11 for the second primary antibody and the appropriate secondary antibody.

13. Wipe the liquid from the slides and apply the mounting medium with DAPI (ab104139, Abcam), then close the slides with coverslips.

14. Secure the coverslips with transparent nail polish.

15. Store the slides at +4 °C until imaging.

Other primary antibodies that we used were Rabbit Iba-1 (PA5-21274, Thermofisher) at 1:250 dilution, Rabbit Glial fibrillary acidic protein GFAP (ab7260) at 1:200 dilution, Rabbit anti-Collagen I (ab34710, Abcam) at 1:300 dilution, and Isolectin GS-IB_4-AlexaFluor^{TM}488 conjugated (121411, Thermofisher) at 1:200 dilution. Secondary antibodies were Alexa 488 anti-rabbit (Thermofisher), and Cy3 anti-mouse (Thermofisher).

2.1.7.2 Imaging

Immunofluorescence labeling of the brain and spinal cord tissues were observed by using Leica DMI8 SP8 Confocal Scanning Microscope. In case of injection point validation, Leica DMi8 LCI microscope was used.

2.1.7.3 Image analysis

We processed the fluorescent images using the LASX program (Leica, Wetzlar, Germany) and exported them as TIF files. For the quantification of PVMs, microglia, and

astrocytes in the brain and spinal cord, brain and spinal cord sections were stained with CD206, Iba1, and GFAP respectively.

Using ImageJ 1.52e (NIH, MD, USA) software, the 20x images taken by the confocal microscope were quantified for CD206, Iba1, and GFAP positive areas.

The TIF pictures were opened in ImageJ software, and the blue channel for DAPI and the red channel for CD206 were separated using the split channels function. The integrated density (IntDen), mean gray value, and percentage of stained area were measured for the cortex and striatum after thresholding. For each animal, at least four images of the cortex and four images of the striatum were analyzed.

In the case of Iba 1 and GFAP staining, the exported TIF pictures were opened with ImageJ software, and the blue channel for DAPI and the green channel for Iba 1 or GFAP were separated using the split channels function of ImageJ. Following thresholding, IntDen, mean grey value, and percentage of stained area were calculated. There were at least 10 images for each staining of the cortex and striatum.

2.1.7.4 Statistical analysis

All statistical analyses were conducted using the GraphPad Prism 10 software (San Diego, USA). Data were presented as Mean±SD if not mentioned otherwise. With the Shapiro Wilk normality test, normality assumptions were made. All groups were compared using the Kruskal-Wallis test. Two groups were compared using the Mann-Whitney U test.

CHAPTER 3

3 Results

3.1 Border macrophages characterization

To delineate CD206-positive cell characteristics and examine potential variations between SOD1-mutated animals and their wild-type littermates, brain and spinal cord tissues were extracted from four mutated rats at their endpoint and four wild-type rats sacrificed at the corresponding age. These tissues underwent staining using a CD206 primary antibody and Cy3 secondary antibody, followed by mounting with DAPI (Figure 3-1).

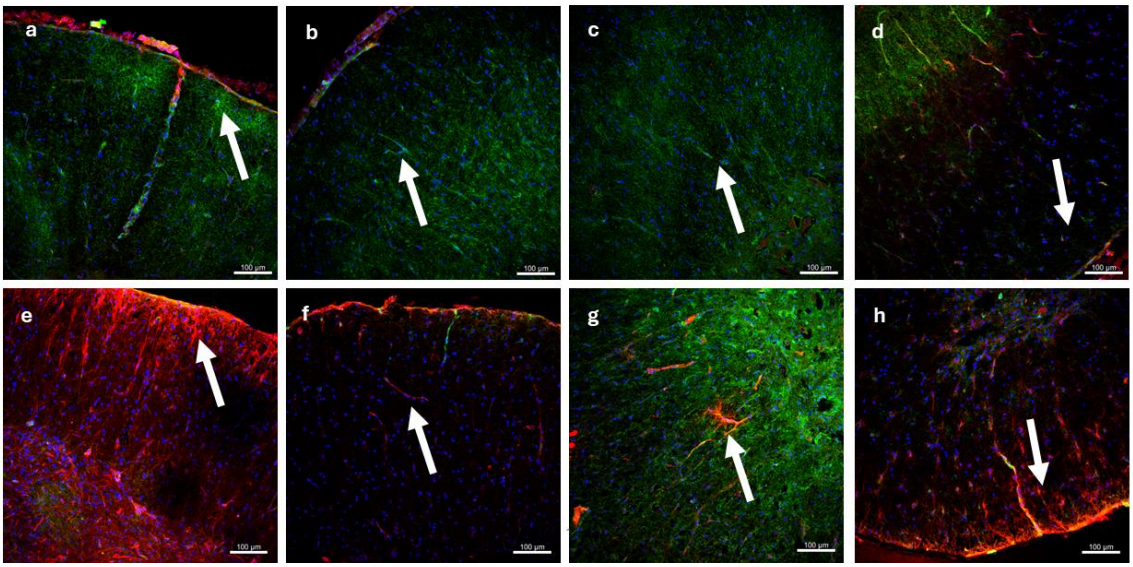

Figure 3-1 The representative images of CD206 IF staining of spinal cord sections. First row images are from WT rats (a, b, c, d). second row images are from SOD1 mutated rats (e, f, g, h). Note the CD206+ cells upregulation in images from SOD1 mutated animals. (CD206 red, IB4 green, DAPI blue. Scale bar is 100 µm).

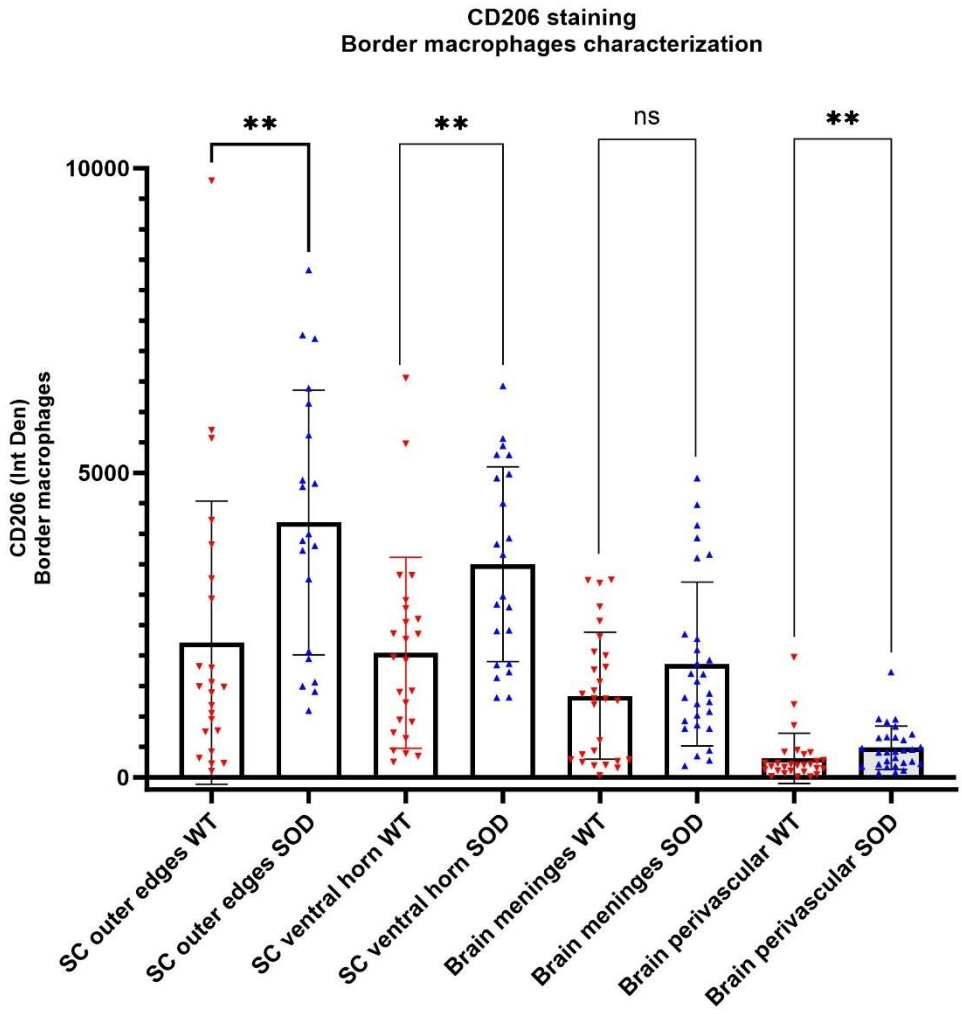

Figure 3-2 The analyses of CD206 stained images of SOD1 and WT animal groups at the end point. Data is presented as Mean±SEM. Dots represent measured IntDen of individual images. SOD1 images have higher CD206 IntDen values than WT in all regions. The difference is significant in spinal cord (SC) outer edges, SC ventral horn, and brain perivascular areas, but in the brain meningeal areas the difference is not statistically different.

As explained before, we analyzed the integrated density parameter of the images red channel (Figure 3-2). The integrated density of $CD206^{+}$ areas was higher in SOD1 mutated animals than their WT littermates, although it was not significant in all regions. The integrated density of CD206 has significantly higher value in the spinal cord outer edges, spinal cord ventral horn, and brain perivascular areas of SOD1 mutated rats than the WT (P=0.0011, P=0.0032, P=0.0031 respectively), while in the brain meningeal regions the difference was not significant (P=0.1726).

3.2 Injection point validation

To confirm the ability of clodronate liposomes to circulate throughout various parts of the central nervous system (CNS) following injection into the cisterna magna, we administered FITC-albumin to the cisterna magna of two wild-type rats. The tissues were stained with CD206 to investigate the colocalization of border macrophages with FITC-albumin.

Microscopy images confirm the FITC-albumin presence in different parts of the CNS including the anterior part of the brain and distal part of the spinal cord. The representative images in Figures 3-3 and 3-4 show the CD206 positive areas are colocalizing with the FITC stained areas in the brain and spinal cord sections.

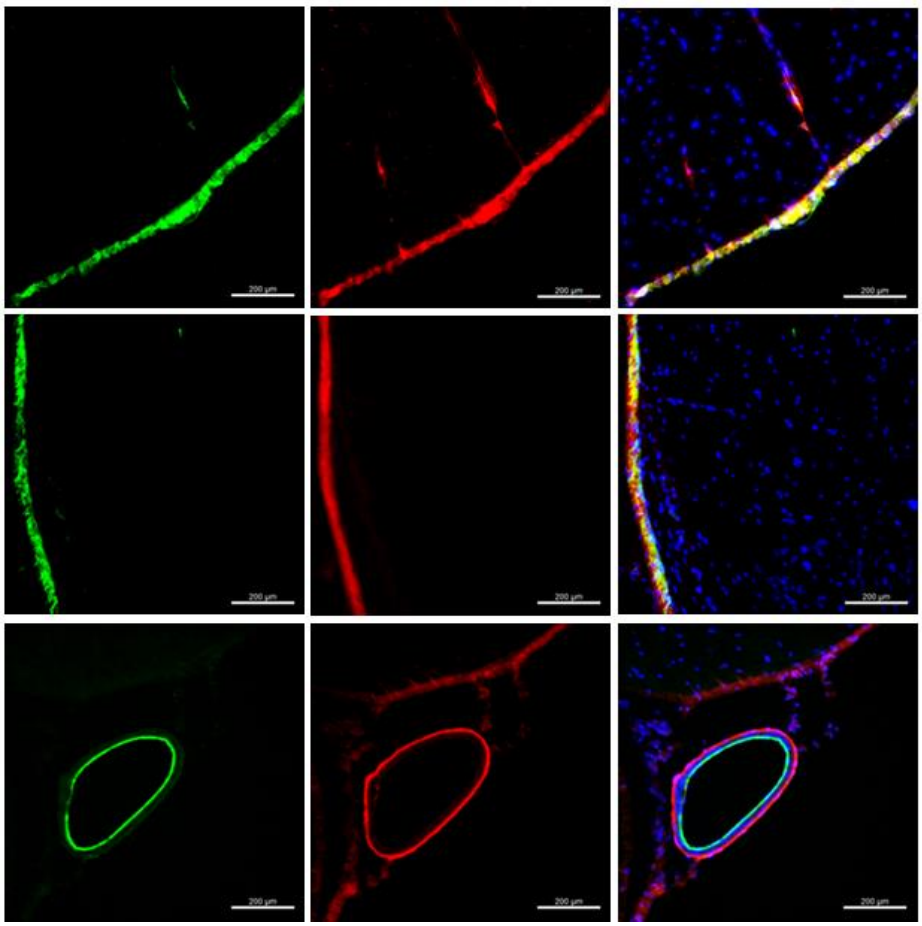

Figure 3-3 CD206 staining from FITC-albumin injected rats' spinal cords. Green, red, and blue channels correspond to FITC-albumin, CD206 and nuclei (DAPI) in order. Note the colocalization of FITC-Albumin and $CD206^{+}$ cells. The scale bar is 200 µm.

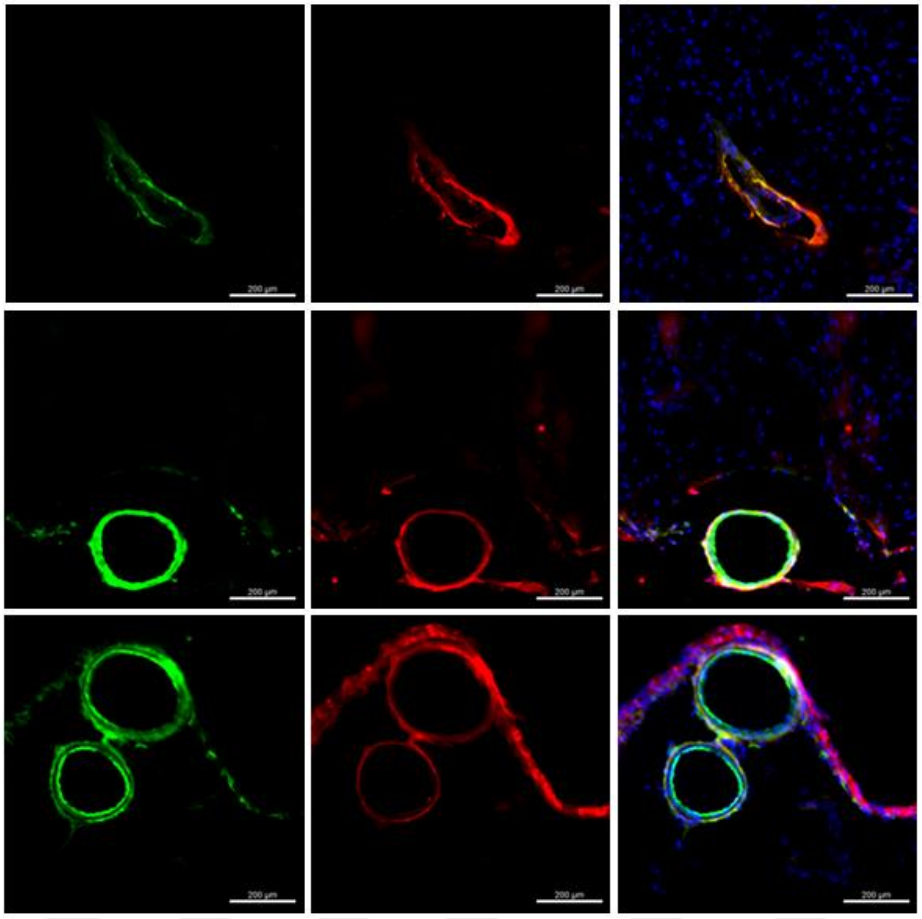

Figure 3-4 CD206 staining from FITC-albumin injected rats' brains. Green, red, and blue channels correspond to FITC-albumin, CD206 and nuclei (DAPI) in order. The scale bar is 200 µm. $CD206^{+}$ cells are colocalizing with FITC-Albumin.

3.3 Validation of PVMs depletion after clodronate liposome injection

As previously mentioned, wild-type rats were sacrificed two weeks after the late single injection of clodronate liposomes. Moreover, rats from the multiple injection group were sacrificed two weeks after the third injection. This experiment aimed to investigate the impact of clodronate liposomes on the population of border macrophages.

The integrated density of CD206 in the brain and spinal cord sections of both depleted and sham WT rats was measured and analyzed.

The image analysis for CD206 positive areas in tissue sections obtained from wild-type animals that received a single injection at day 160 after birth is presented in Figure

3-5. Despite observing a decrease in CD206 positive macrophages in the depleted group in all regions, such as brain borders, brain perivascular, spinal cord borders, and spinal cord perivascular, the differences with the sham group are not statistically significant (P Values are 0.2514, 0.4274, 0.2448, and 0.7961, respectively).

In the multiple injection experiment, the CD206 positive areas exhibit a decrease in all locations, as indicated in the graph of Figure 3-6. Notably, there is a significant decrease in the spinal cord borders (both outer edges and central canal) and brain borders of the depleted group (P value < 0.0001, P value=0.0452 in order). However, the observed differences are not statistically significant for the brain perivascular, and spinal cord perivascular (P values are 0.3829 and 0.4634 in order).

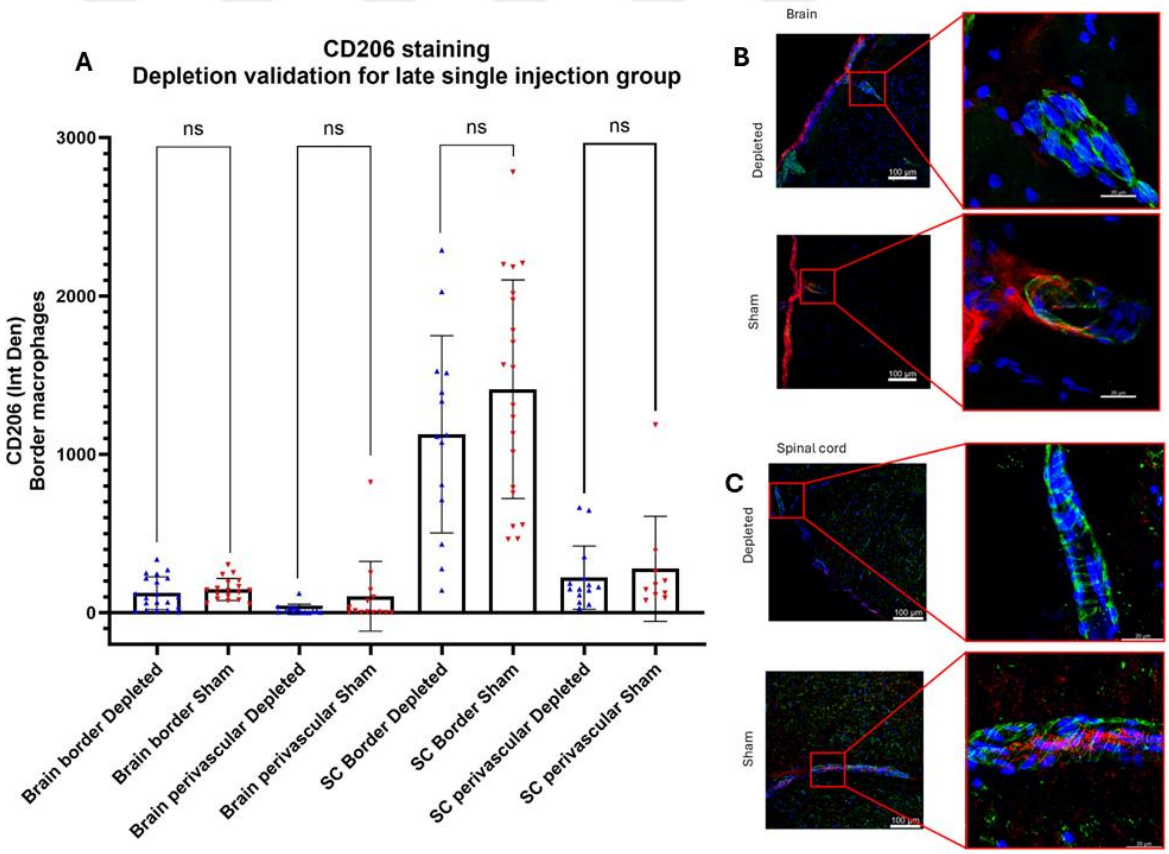

Figure 3-5 The analysis of CD206 stained images of depleted and sham WT rats received late single injection. A) The IntDen of the CD206 stained area. Data is presented as Mean±SEM. IntDen is lower in all regions of depleted group, although the difference is not statistically significant (P values are 0.25, 0.42, 0.24, and 0.79 from left to right in order). B, C) representative images from Brain and

Spinal cord of depleted and sham groups respectively. Note the difference between red channel in depleted and sham images. Scale bar is 100µm in 20x images and 20µm in zoomed images. CD206 is red, IB4 is green, and nuclei is blue (DAPI).

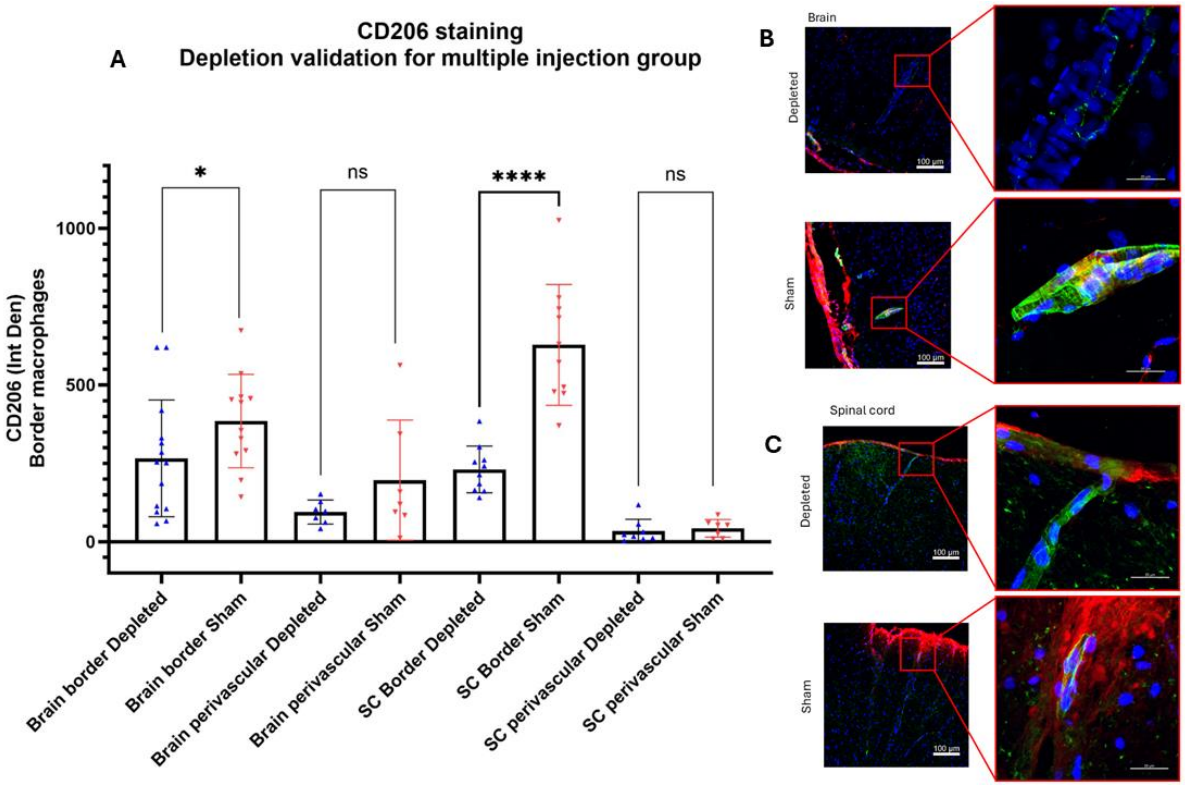

Figure 3-6 The analysis of CD206 stained images of depleted and sham WT rats of multiple injection experiment. A) The IntDen of the CD206 stained area. Data is presented as mean±SEM. IntDen is lower in all regions of the depleted group. The depletion is significant in Brain borders and spinal cord borders (P values are 0.0452 and <0.0001 respectively), although the difference was not statistically significant for brain and spinal cord perivascular (P values are 0.3829 and 0.4634 in order). B, C) representative images from Brain and Spinal cord of depleted and sham groups respectively. Note the difference between red channel in depleted and sham images. Scale bar is 100µm in 20x images and 20µm in zoomed images. CD206 is red, IB4 is green, and nuclei is blue (DAPI).

3.4 Behavior test

3.4.1 Weight changes

From the day of injection to the endpoint, the weights of the animals were documented twice a week and arranged in XY tables. Simple linear regression was employed to assess group comparisons. To mitigate the influence of gender, the weights were normalized based on their initial recorded weights.

Due to the early single administration of the Clodronate/PBS loaded liposome, the depleted group showed higher average weight from the injection day to the symptomatic stage beginning. During the symptomatic stage until the end point the depleted and sham curves intersect each other and their difference decreased (Figure 3-7).

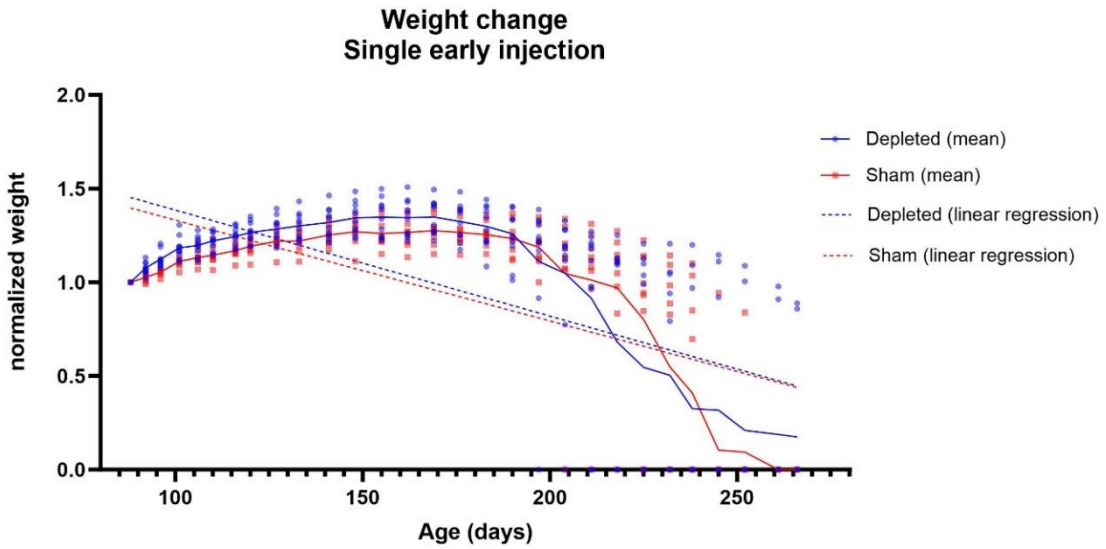

Figure 3-7 weight of the animals in early single injection experiment. Continuous lines show the average weight of the groups, while the dashed lines are simple linear regression of the continuous lines. Animals' weights are normalized to their first recorded weight.

In the multiple injection experiment, despite the repeated injections of clodronate loaded liposomes and depletion of CD206 positive cells, it appears that the weight change of the depleted group is comparable to that of the sham group from the first injection day to the symptomatic phase onset. During the symptomatic stage the depleted group shows higher average weight compared to the sham group (Figure 3-8). The blue dashed line representing the depleted group is less steep than the red line representing the sham group (Slopes are -6.575×10^{-3} and -7.247×10^{-3} in order). This indicates a subtle change in weight within the depleted group in comparison to the sham group.

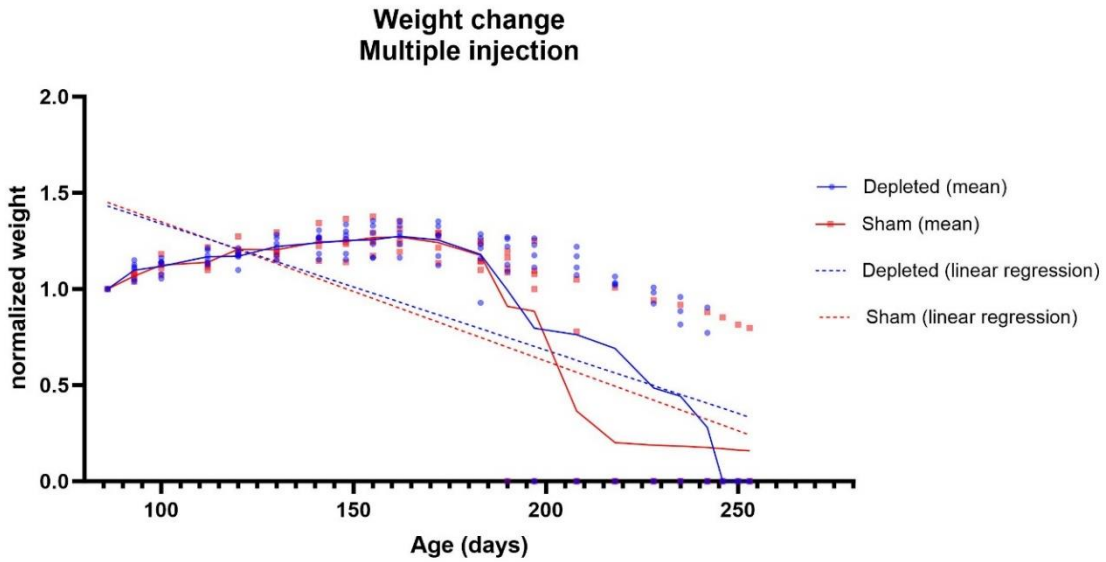

Figure 3-8 weight of the animals in multiple injection experiment. Continuous lines show the average weight of the groups, while the dashed lines are simple linear regression of the continuous lines. Animals' weights are normalized to their first recorded weight.

In the late single experiment animals received clodronate loaded liposomes maintained their weight for a longer period of time than those received PBS loaded liposomes as the sham treatment (Figure 3-9). Both groups had similar average weights during the symptomatic stage and their average cures intersected each other several times.

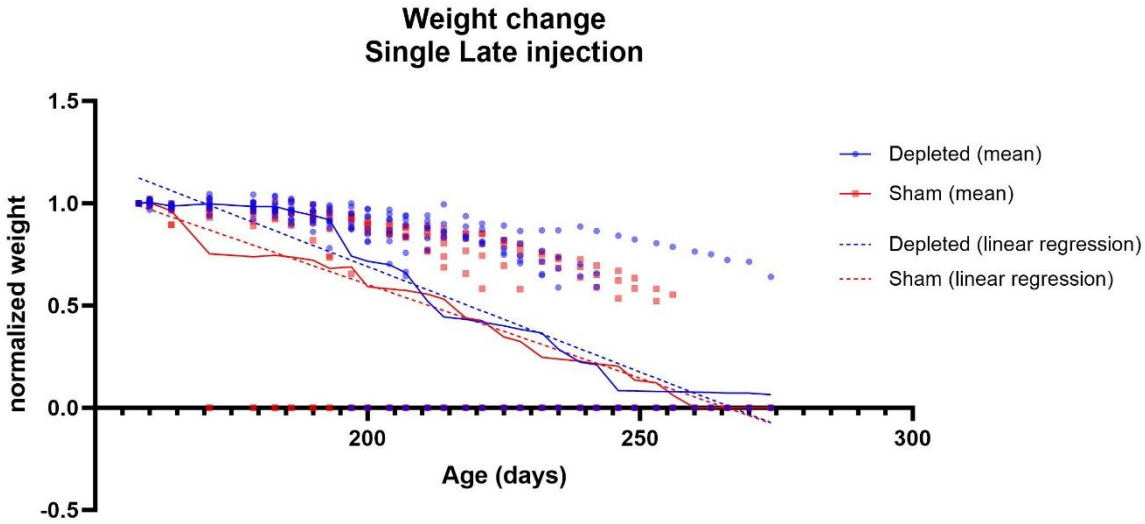

Figure 3-9 weight of the animals in the late single injection experiment. Continuous lines show the average weight of the groups, while the dashed lines are simple linear regression of the continuous lines. Animals' weights are normalized to their first recorded weight.

3.4.2 Locomotor activity tests

To determine the total score for each animal for every week, individual scores from different items were summed, resulting in a numerical value ranging from 0 to 33. These aggregated data were then inputted into an XY table to generate curves based on the mean values of the respective groups. Subsequently, the slopes of these curves were calculated using simple linear regression.

In the early single injection group, animals underwent continuous monitoring and assessment over a span of 23 weeks. The results of the tests revealed comparable performances between the two groups (Figure 3-10). Notably, the slopes of the red line representing the sham group and the blue line depicting the depleted group were found to be closely aligned at -1.552 and -1.541, respectively.

Despite the sham group having a higher average score during the symptomatic stage, the depleted group exhibited a higher average score during the last month of the experiment. This was due to two animals from the depleted group showing a notable extension in survival, exceeding the duration lived by the last surviving animal from the sham group by one week. It appears that the average score of the sham group decreased with a delay compared to the depleted group. However, once the decline in the curve began, the slope of the sham group's curve was steeper than that of the depleted group.

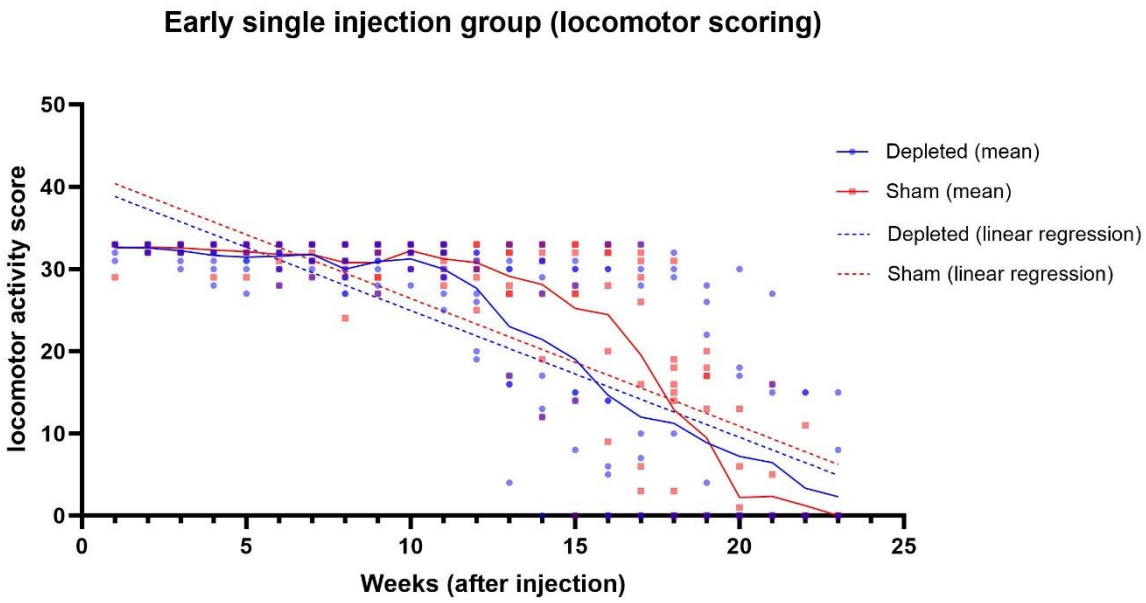

Figure 3-10 The locomotor activity test results from the early single injection experiment are illustrated. Individual scores of the animals are represented by dots, while the continuous curves depict the group averages. Dashed lines indicate the simple linear regression of the curves. The slopes for the depleted and sham groups are -1.541 and -1.552, respectively.

The multiple injection group underwent scoring from day 85 to day 250 after birth on a weekly basis. Data spanning twenty-two consecutive weeks were collected and analyzed, with the results presented graphically. Individual data points are represented by dots, while lines connect the mean values of each group, illustrating the slope of the curves (Figure 3-11).

Initially, in the first week following the first injection, scores for both the depleted and sham groups were comparable. However, as the study progressed towards the endpoint, the depleted group exhibited higher scores. The slope of the blue line (representing the depleted group) is -1.534, which is less steep than the red line (representing the sham group) with a slope of -1.699.

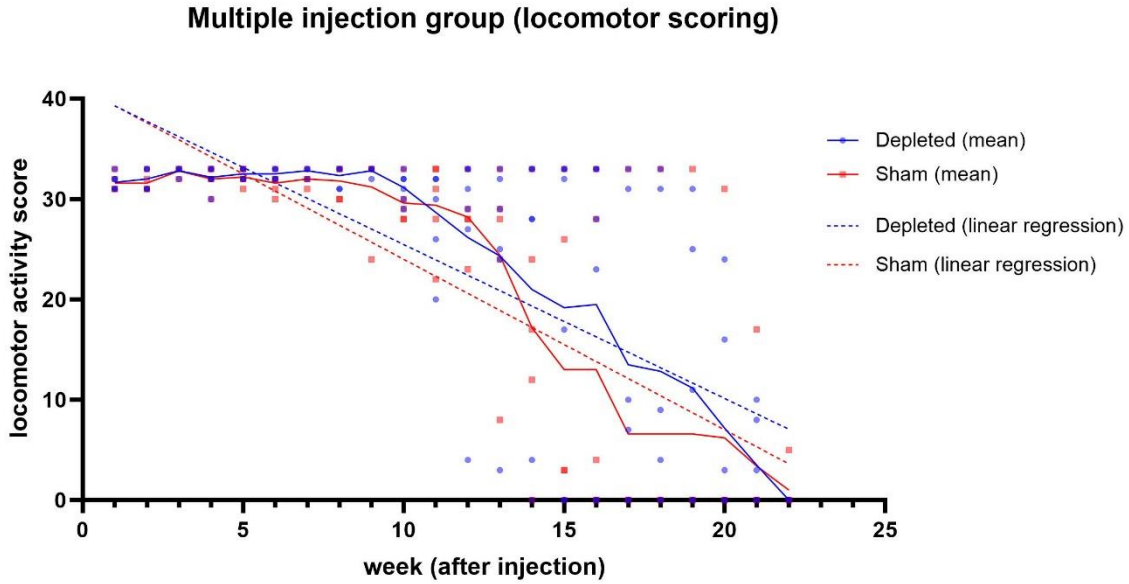

Figure 3-11 The locomotor activity test results from the multiple injection experiment are displayed. Individual scores of the animals are depicted by dots, while the continuous curves represent the group averages. Dashed lines indicate the simple linear regression of the curves. The slopes for the depleted and sham groups are -1.534 and -1.699, respectively. It's worth noting the higher average score of the depleted group in most of the scoring sessions.

Animals in the single late injection group were assessed weekly, commencing four days after injection (day 164 after birth), and continuing for 16 consecutive weeks until the study's endpoint. Similar to the previously described method, data analysis was conducted using the same approach, and the results were visually represented.

In the graphical representation (Figure 3-12), despite the steeper slope of the blue line (depleted group) at -2.449 compared to the red line (sham group) with a slope of -2.200, the depleted group consistently displayed higher scores throughout the entire experimental period. Additionally, noteworthy is the observation that one animal from the depleted group survived three weeks longer than the last animal in the sham group.

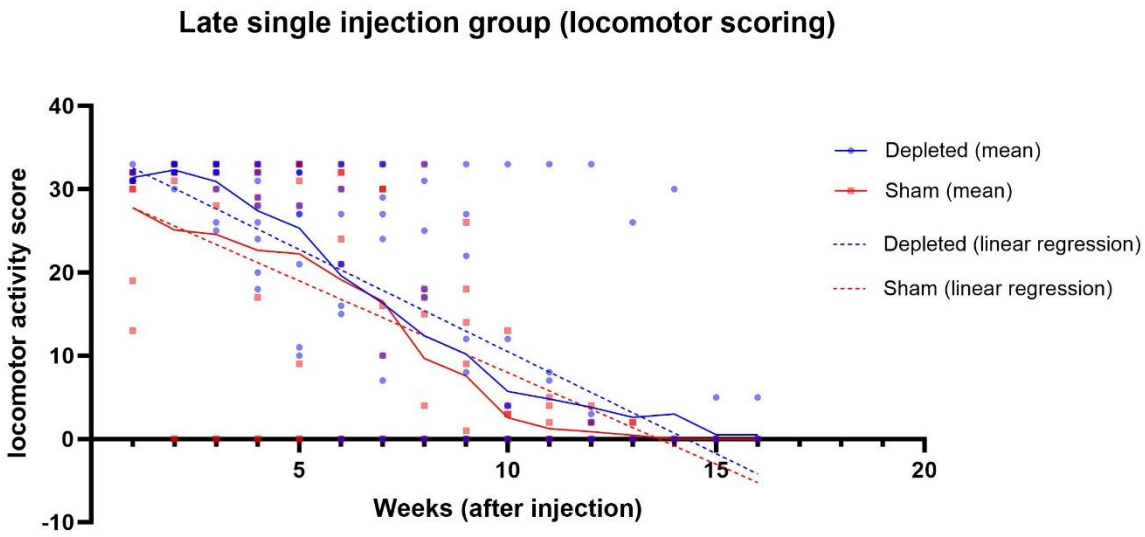

Figure 3-12 The locomotor activity test results from the late single injection experiment are depicted. Individual scores of the animals are represented by dots, while the continuous curves represent the group averages. Dashed lines indicate the simple linear regression of the curves. The slopes for the depleted and sham groups are -2.449 and -2.200, respectively. It's noteworthy that despite the steeper linear regression line for the sham group, the depleted group exhibited higher average scores in most of the scoring sessions.

3.4.3 Ladder rung test

The ladder rung test was conducted on a weekly basis for all the animals, as previously detailed. Each pass was precisely analyzed by counting the number of faults and the total steps, allowing for the calculation of both the percentage of correct steps and the average of three repetitions. The resulting graphs display individual data points represented by dots. The groups average ladder rung score trends are shown by continuous curves, while

the dashed lines illustrate the outcomes of the simple linear regression test, indicating the slope of data changes for each group.

In the case of the early single injection group, the assessment period spanned from day 160 to 250, covering 80 days post-injection until the endpoint. The blue line, representing the depleted group, exhibited a less steep slope compared to the red line (slopes of -7.159 and -9.723, respectively), indicating a slower progression of motor deficit symptoms (Figure 3-13). Notably, while the sham group initially demonstrated better performance, as the study approached its endpoint, the average score of the depleted group surpassed that of the sham group. In the last week of scoring, a noteworthy observation emerged – only one animal from the depleted group retained the ability to traverse the rungs.

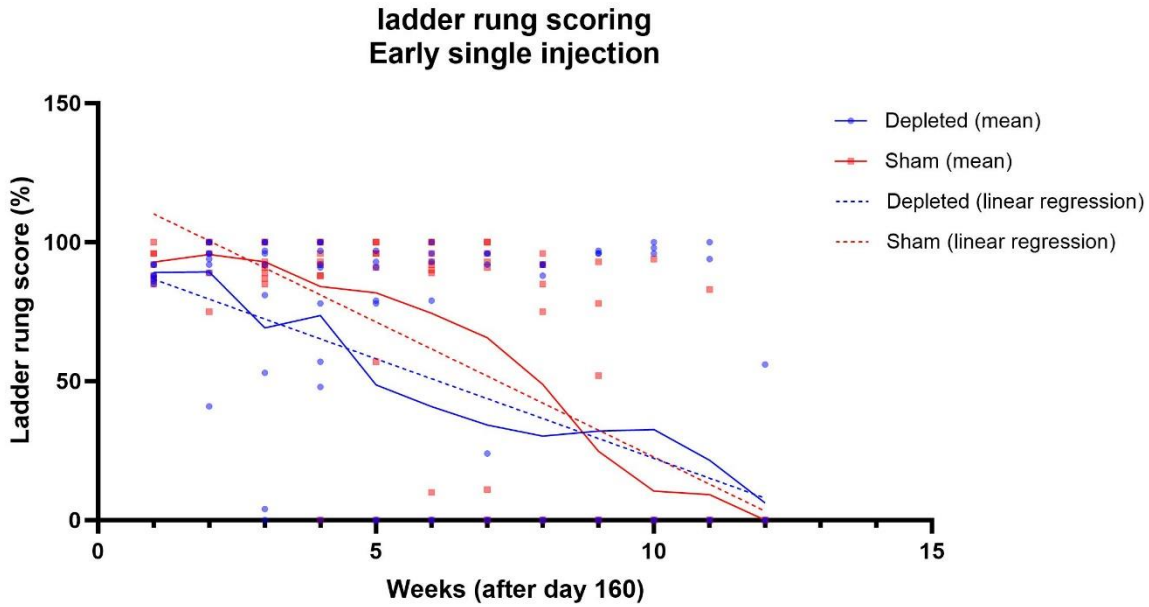

Figure 3-13 The ladder rung test results from the early single injection experiment are presented. The curves represent the average percentage of correct steps for the depleted and sham groups (blue and red, respectively). While the sham group exhibited a higher average in most of the scoring sessions, the depleted group's average declined with a less steep slope.

The animals in the multiple injection group underwent weekly testing sessions spanning approximately from day 110 to day 240, totaling 18 sessions. Throughout this testing period, the depleted group consistently exhibited a superior average score compared to the sham group in most sessions (Figure 3-14). The graph depicting the results reveals distinct trends, with the blue line representing the depleted group displaying a less steep slope (-5.580), in contrast to the steeper slope observed in the red line representing the sham group (-5.806).

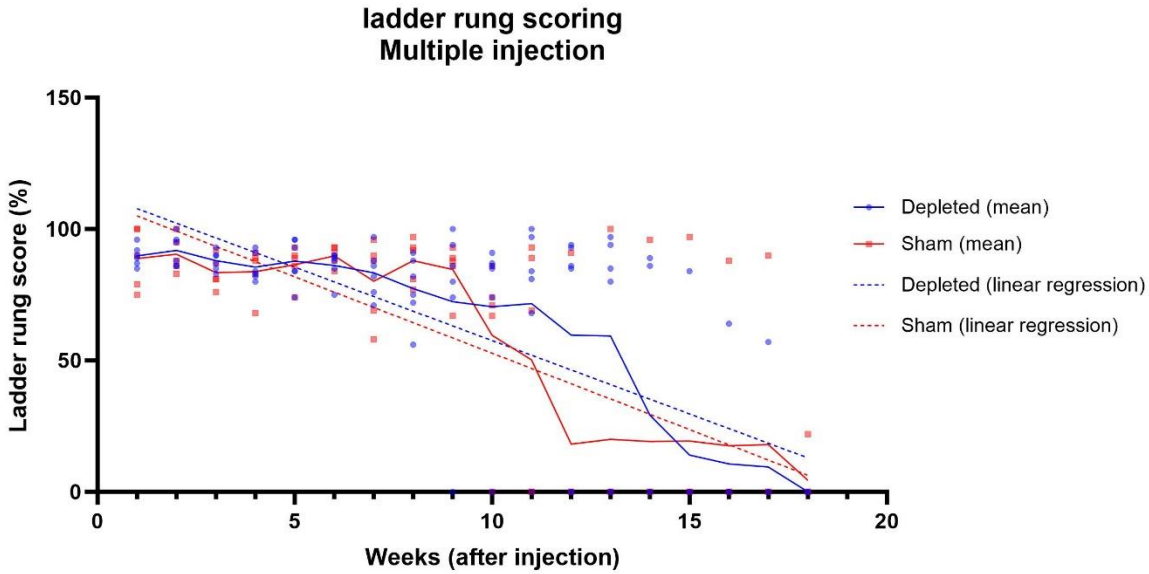

Figure 3-14 The ladder rung test results from the multiple injection experiment are presented. The curves depict the average percentage of correct steps for the depleted and sham groups (blue and red, respectively). The depleted group demonstrated a higher average in most of the testing sessions, with the blue line showing a less steep slope compared to the red line (-5.580 and -5.806, respectively). This confirms a milder symptomatic stage for the depleted group.

During the late single injection experiment, animals underwent testing sessions for a duration of 12 weeks, spanning approximately from day 165 to day 255. In a pattern reminiscent of the multiple injection experiment, the depleted group consistently demonstrated superior performance in the majority of test sessions (Figure 3-15). Interestingly, despite the steeper slope of the blue line representing the depleted group (-8.513) compared to the red line representing the sham group (-8.159), the depleted group exhibited better overall performance.

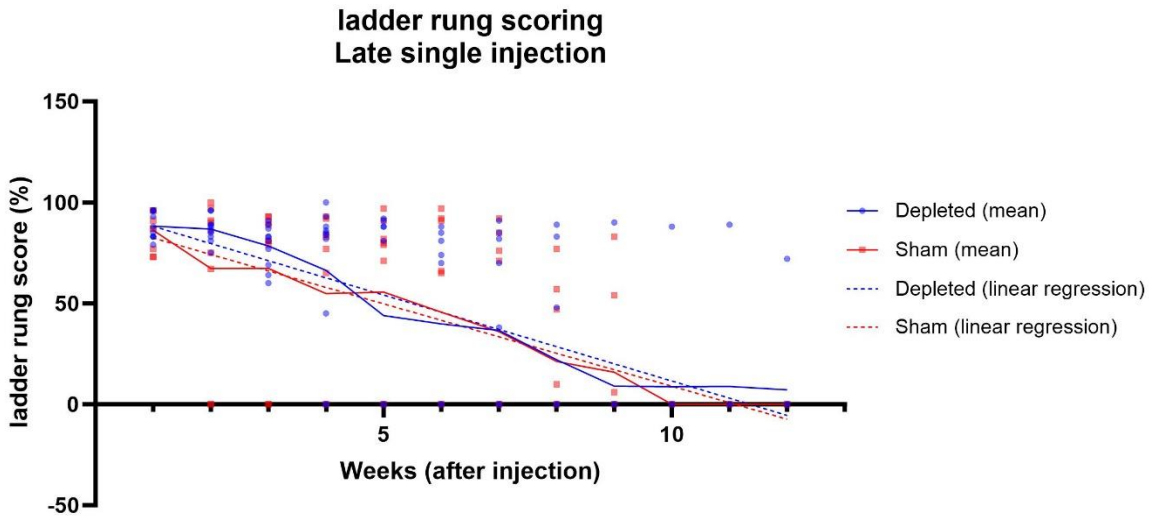

Figure 3-15 The ladder rung test results from the late single injection experiment are displayed. The curves show the average percentage of correct steps for the depleted and sham groups (blue and red, respectively). The depleted group exhibited a higher average in testing sessions of the first month after injection. However, the red line displayed a less steep slope compared to the blue line (-8.159 and -8.513, respectively). This indicates a delayed symptomatic stage in the depleted group.

3.4.4 Survival and probability of remaining healthy (pre symptomatic stage)

To assess the impact of depleting the BAMs on survival, we utilized Kaplan-Meier analysis. Survival graphs were generated based on the animals' ages at the time of termination for each of the three experiments individually. The Gehan-Breslow-Wilcoxon test was employed for data analysis.

Furthermore, we utilized the recorded weights of the animals to create Kaplan-Meier graphs in an alternative manner. The peak weight was identified as the onset of the pre-symptomatic stage. For each rat, we determined the age at which it reached this stage. Subsequently, Kaplan-Meier graphs were generated by defining the day when the animal was at its peak weight as the event. These curves were plotted separately for the single early injection, multiple injections, and single late injection groups. Once again, the Gehan-Breslow-Wilcoxon test was utilized for data analysis.

The survival analysis for the single early injection experiment did not indicate a statistical difference between the depleted and sham groups (Figure 3-16 A). The numerical data of peak weight age depicted in the graph reveals that, although a trend was observed wherein most animals from the depleted group reached the pre-symptomatic stage later than those in the sham group, this difference did not achieve statistical significance (Figure 3-16 B, P value = 0.1922).

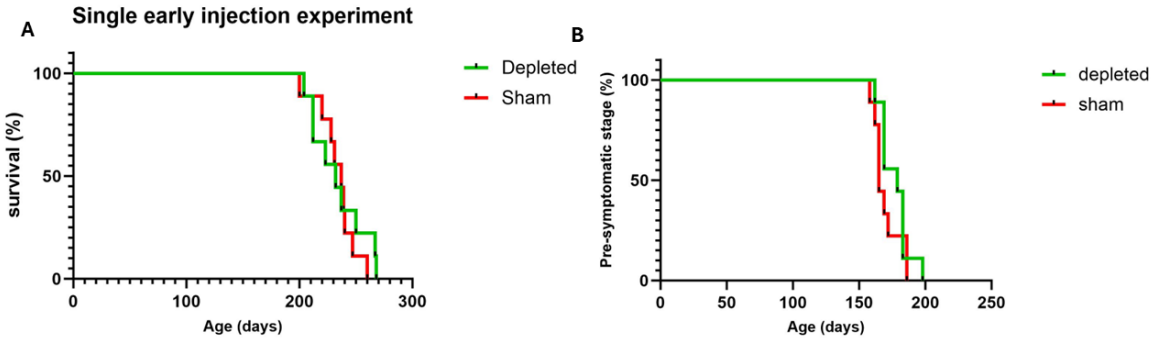

Figure 3-16 Survival results for the early single injection experiment. A) Kaplan-Meier analysis for overall survival showed no significant difference between groups (P value=0.93). B) Kaplan-Meier analysis for the probability of not

reaching the symptomatic phase yielded a P value of 0.192, indicating no statistically significant difference between the groups. The Gehan-Breslow-Wilcoxon test was used for data analysis.

In the multiple injection experiment, the survival analysis does not reveal a notable difference between the depleted and sham groups (Figure 3-17 A, P value= 0.716). However, a consistent trend is observed where the depleted group exhibits a lower probability of reaching the pre-symptomatic stage compared to the sham group. Importantly, statistical analysis reveals that this difference is significant, with a p-value of 0.0316 (Figure 3-17 B).

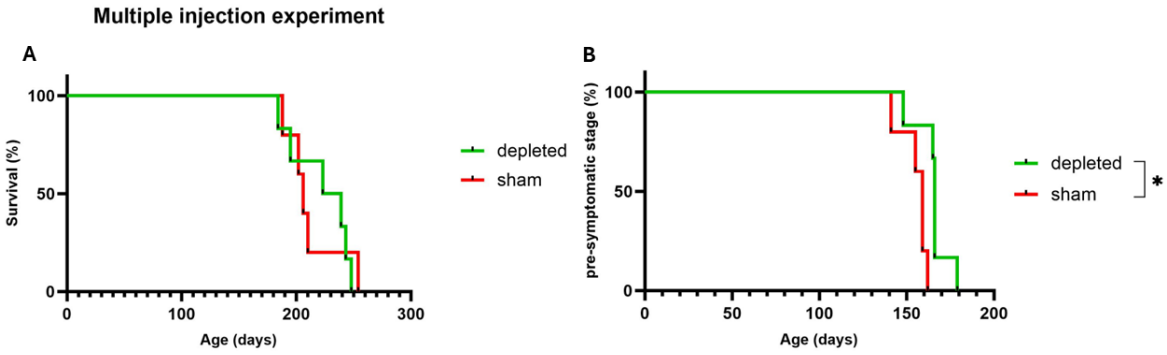

Figure 3-17 Survival results for the multiple injection experiment. A) Kaplan-Meier analysis for overall survival showed no significant difference between groups (P value=0.716). B) Kaplan-Meier analysis for the probability of not reaching the symptomatic phase revealed a statistically significant difference between the depleted and sham groups (P value=0.0316), analyzed using the Gehan-Breslow-Wilcoxon test.

In the late single injection experiment, although the difference between the depleted and sham groups did not reach statistical significance regarding the likelihood of reaching the presymptomatic stage, the calculated p-value of 0.0554 is notably close to the threshold of significance (Figure 3-18 B). Like the single early and multiple injection experiments, the survival analysis did not show a significant difference (Figure 3-18 A).

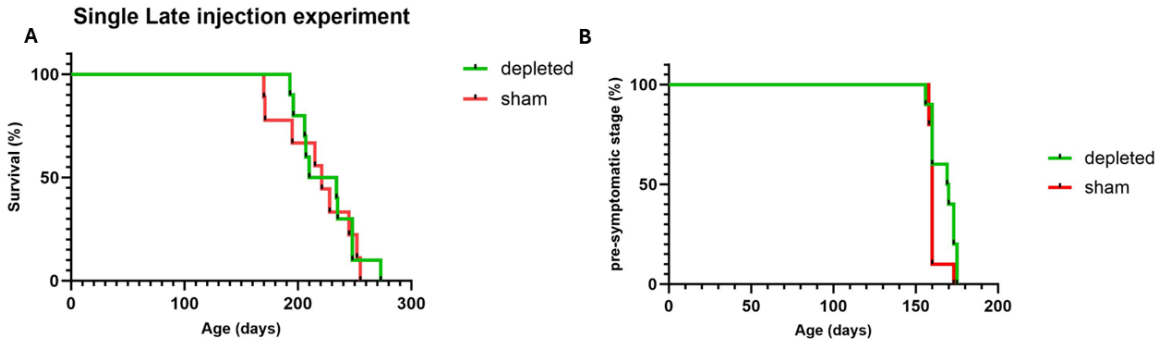

Figure 3-18 Survival results for the late single injection experiment: A) Kaplan-Meier analysis for overall survival showed no significant difference between groups (P value=0.745). B) Kaplan-Meier analysis for the probability of not reaching the symptomatic phase revealed no statistically significant difference between the depleted and sham groups. However, the P value approached the threshold for significance (P value=0.055), analyzed using the Gehan-Breslow-Wilcoxon test.

3.5 Immunofluorescence staining

3.5.1 CD206 staining

As described previously, CD206 primary antibody and CY3 secondary antibody were used to stain tissues from the multiple injections and single late injection groups. We took confocal images from the striatum and the cortex of the brains, and the ventral horn of the spinal cords (lumbar sections). There were at least four images taken from the striatum and the cortex, and eight images taken from the ventral horn of each animal. Staining was performed at the end of experiments and there is no longitudinal data.

The depleted groups show greater densities of perivascular macrophages in the ventral horn of the lumbar spinal column compared with the sham group. In the multiple injection experiment, the difference is statistically significant (Figure 3-19 A), whereas in the late single injection experiment, it is not statistically significant (Figure 3-20 A).

In both experiments, the CD206 positive cells have increased in the cortex of the depleted group compared to the sham group, but the difference is not statistically significant.

Multiple injection experiment animals showed a different pattern in terms of CD206 cell density in the striatum. A significant reduction in CD206 density was observed in the depleted animals in the multiple injection group, compared to the sham multiple injection group (3-19 A). Despite this, the striatum of the single injection experiment showed the same pattern as the cortex and ventral horn (3-20 A).

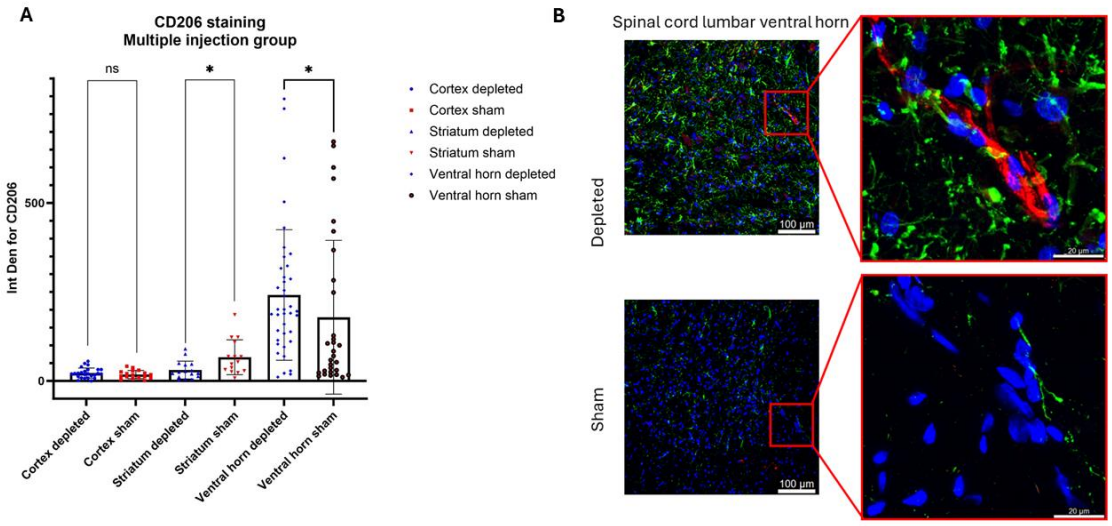

Figure 3-19 The analysis of CD206 stained images from depleted and sham SOD1 rats in the multiple injection experiment revealed the following: A) The IntDen of the CD206 stained area: In the ventral horn, IntDen was significantly higher in the depleted group compared to the sham group (P value=0.0161). Surprisingly, in the striatum, IntDen was higher in the sham group (P value=0.0106). However, there was no meaningful difference in IntDen observed in the brain cortex (P value=0.3877). B) Representative images from the lumbar section of the spinal cord showed notable differences in the red channel between the depleted and sham groups. Scale bars are 100µm and 20µm respectively for 20x and zoomed images, with CD206 stained in red, GFAP in green, and nuclei in blue (DAPI).

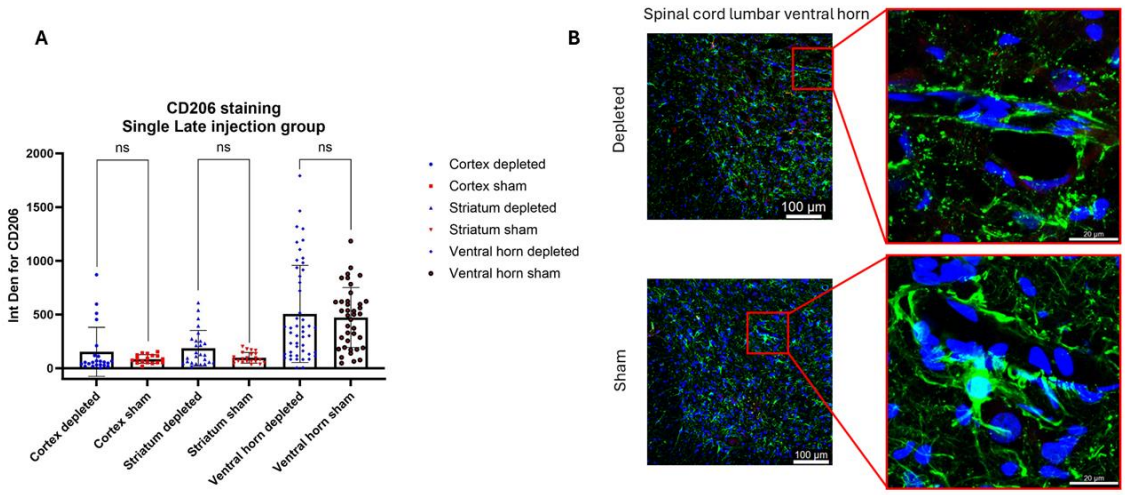

Figure 3-20 The analysis of CD206 stained images from depleted and sham SOD1 rats in the late single injection experiment revealed the following: A) The IntDen of the CD206 stained area: In the ventral horn, striatum, and cortex of depleted group has upregulated but the difference with sham group is not statistically significant (P values are 0.5896, 0.1443, and 0.2653 respectively). B) Representative images from the lumbar section of the spinal cord do not show notable differences in the red channel between the depleted and sham groups. Scale bars are 100µm and 20µm respectively for 20x and zoomed images, with CD206 stained in red, GFAP in green, and nuclei in blue (DAPI).

3.5.2 GFAP staining

To study the astrogliosis, the tissues were stained by GFAP (Alexa Flour 488 as secondary antibody).

In the multiple injection experiment, the brain tissues from both depleted and sham animals showed almost equal levels of astrogliosis. As a result of PVMs depletion, the density of GFAP in the ventral horn of the depleted group was significantly higher than that in the sham group. There is a statistically significant difference between the two groups with a P value less than 0.0001 (Figure 3-21). Representative images are the same as the CD206 staining part (figure 3-19).

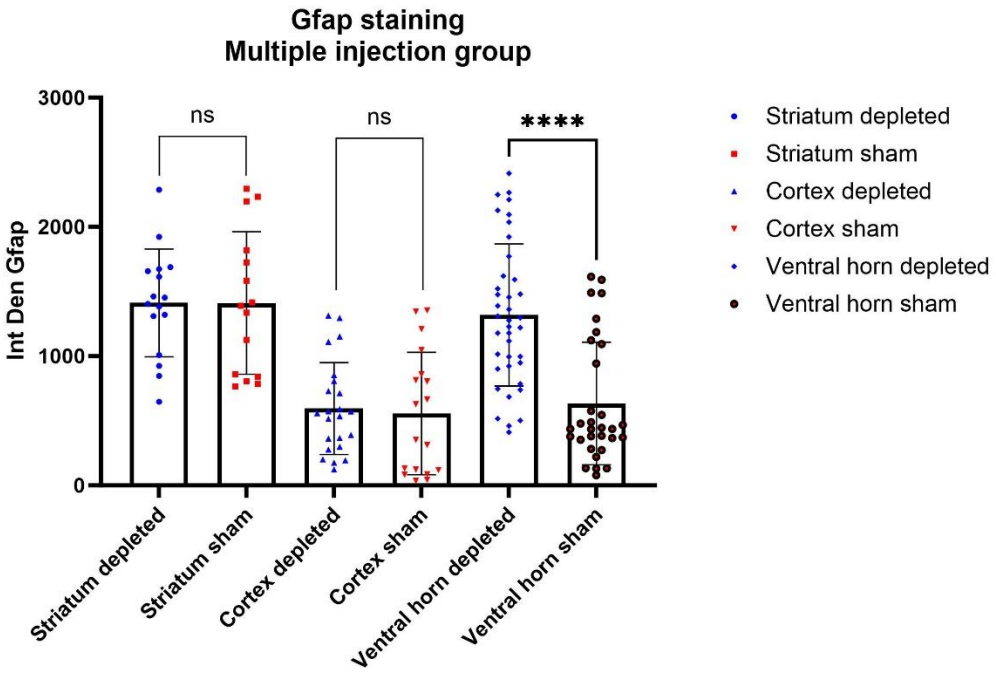

Figure 3-21 The analysis of GFAP stained images from depleted and sham SOD1 rats in the multiple injection experiment revealed the following: The IntDen of the GFAP stained area: In the ventral horn of depleted group has upregulated significantly compared to sham group (P value<0.0001). In the striatum and cortex of depleted group the difference is not statistically significant with sham group (P values are 0.9966, 0.5411 respectively).

In the case of the late single injection experiment, although there was more astrogliosis in the cortex and striatum of the depleted animals than in the sham animals, the difference was not statistically significant (P values are 0.3423 and 0.3187 respectively). The IntDen of GFAP in the ventral horn was almost equal (P value=0.8289) (Figure 3-22). Representative images are the same as the CD206 staining part (Figure 3-20).

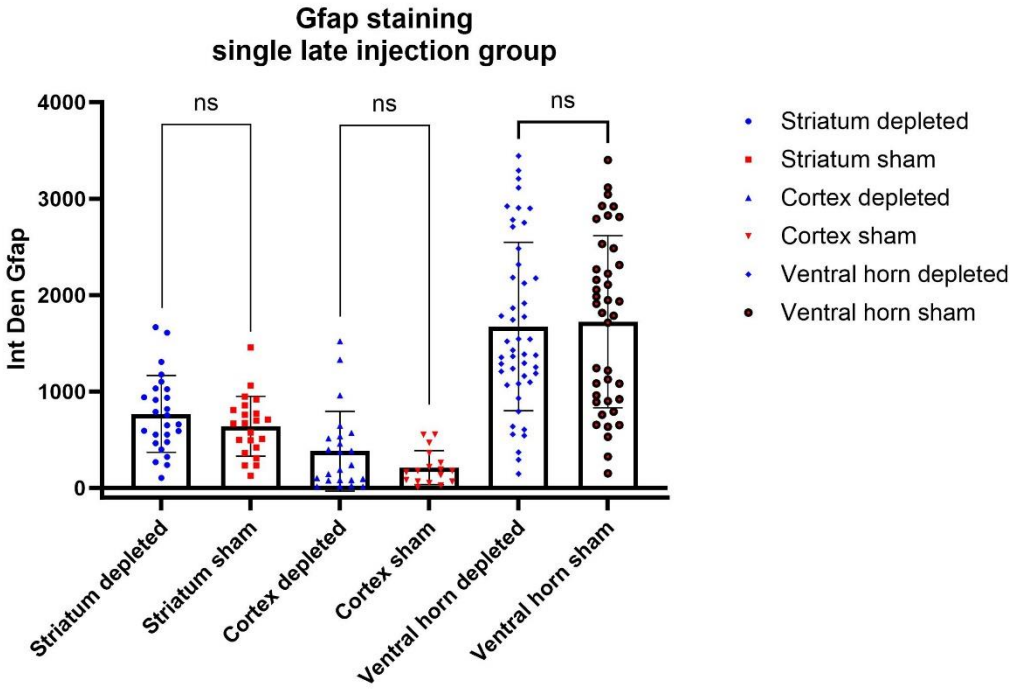

Figure 3-22 The analysis of GFAP stained images from depleted and sham SOD1 rats in the late single injection experiment revealed the following: The IntDen of the GFAP stained area in the ventral horn, striatum, and cortex of depleted group is not significantly different with sham group (P values are 0.8289, 0.3187, and 0.3423 respectively).

3.5.3 Iba 1 staining

Microglia activation was examined by staining the brain and lumbar section of the spinal cord with Iba 1 (Alexa flour 488 was used as a secondary antibody). There is no significant difference between the activation of microglia in the brains of depleted and sham animals in either experiment (multiple and late single injection experiments).

In both experiments, depleted animals showed higher activation of microglia in the lumbar ventral horn than in sham groups. There is a statistically significant difference, P value is 0.035 for multiple injections (Figure 3-23) and 0.0042 for late single injections (Figure 3-24).

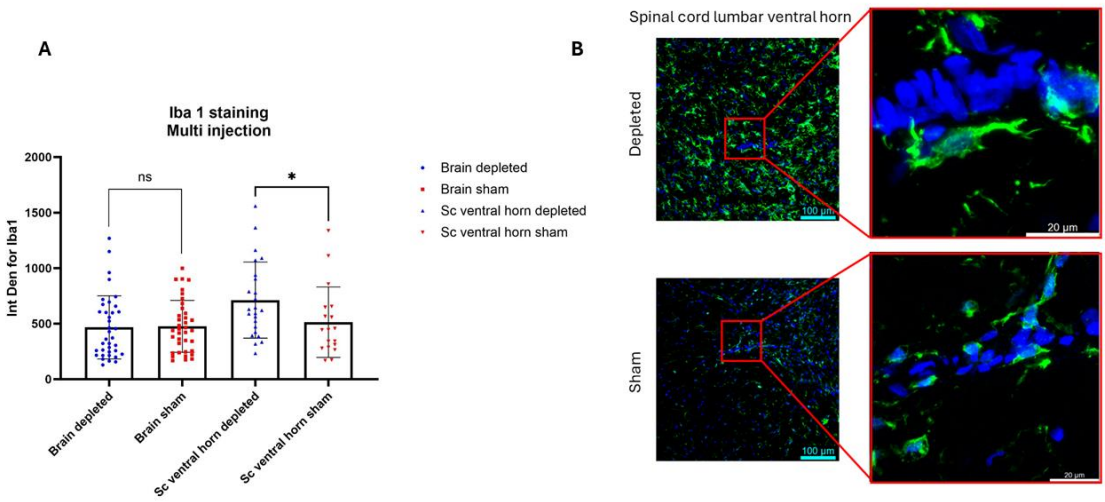

Figure 3-23 The analysis of Iba 1 stained images from depleted and sham SOD1 rats in the multiple injection experiment revealed the following: A) The IntDen of the Iba 1 stained area: In the ventral horn of depleted group has upregulated significantly with a P value of 0.035. B) Representative images from the lumbar section of the spinal cord. Note the difference of green channel that is Iba 1 stained areas. Scale bars are 100µm and 20µm respectively for 20x and zoomed images, with Iba 1 in green and nuclei in blue (DAPI).

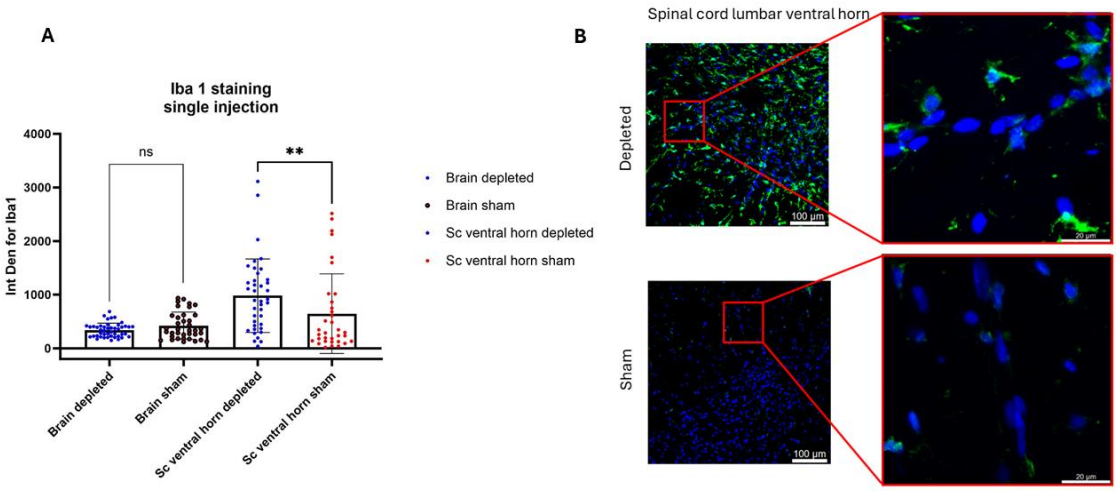

Figure 3-24 The analysis of Iba 1 stained images from depleted and sham SOD1 rats in the late single injection experiment revealed the following: A) The IntDen of the Iba 1 stained area: In the ventral horn of depleted group has upregulated significantly with a P value of 0.0042. the IntDen of Iba 1in the brain sections is not significantly different (P value=0.4694). B) Representative images from the lumbar section of the spinal cord. Note the difference of green channel that shows Iba 1 stained areas. Scale bars are 100µm and 20µm respectively for 20x and zoomed images, with Iba 1 in green and nuclei in blue (DAPI).

Chapter 4

4 Discussion

There is no complete explanation for the etiopathogenesis of ALS based on genetic mutations or environmental risk factors alone.

The purpose of this study is to investigate the effects of BAMs on ALS by investigating the effects of their depletion on the progression of the disease, weight fluctuations, and locomotor activity in rats. Moreover, we examined the activation of microglia, astrocytes, and BAMs at the late stage of ALS in the depletion and sham groups.

To assess the role of BAM in ALS, we utilized clodronate-loaded liposomes, and injected it into the cisterna magna of SOD1 mutated rats. This procedure aimed to deplete resident macrophages in the brain and spinal cord borders. A sham-operated group underwent a similar procedure but received liposomes loaded with PBS as control for the potential effects of liposomes and surgical complications.

Fifty-nine SOD1 mutant rats and 26 WT rats with Sprague Dawley backgrounds were used in this study. SOD1 rats were monitored until the end of the study, human end point. For the purpose of comparing the BAM populations of the WT rats with the SOD1 rats, validating the injection site, and confirming depletion, WT rats were included in the study.

Immunofluorescent staining confirmed the presence of CD206-positive cells in vicinity of the vessels in the SOD1 model. This findings are in line with a previous study of single-cell RNA-sequencing of non-neuronal cells in the mouse cerebral cortex (Jeong et al., 2022). We detected that in comparison to WT rats, CD206 positive cells were significantly more abundant in the ventral horn and the outer edges of the spinal cord and brain perivascular areas of SOD1 mutant rats. Although the macrophages were more populated in the SOD1 brain meninges as well, the difference was not statistically significant. This suggests that macrophages associated with the CNS borders are increased in response to ALS, especially in the ventral horn. These findings align with the results from previous research investigating the role of PVM in ALS, which was conducted using a SOD1 mouse model. (Adachi et al., 2023). Adachi et al. conducted a study examining alterations in the number and heterogeneity of PVMs in the spinal cord

of SOD1 mice, comparing it with samples from wild-type mice at various time points, spanning from the pre-symptomatic stage to the study endpoint. Their findings revealed that in the pre-symptomatic animals, both the number and phenotype of PVMs in the SOD1 mice resembled those in the WT mice. However, as the disease progressed, there was an increase in the number of PVMs, and their phenotype transformed from the anti-inflammatory Lyve1$^+$ type to the pro-inflammatory MHCII$^+$ type.

To directly demonstrate the effects of BAMs to ALS pathophysiology, we used clodronate loaded liposome. Since clodronate passage to CNS is limited, we have used cisterna magna injection. First, we examined the extent to which an injection into the animal's cisterna magna could reach different locations within the CNS. For this purpose, we administered FITC-Albumin into the cisterna magna of two wildtype rats. One hour later, the rats were euthanized, and their brains and spinal cords underwent processing for immunofluorescence staining with CD206 antibody. The resulting images demonstrated that FITC-Albumin successfully reached the CD206$^+$ cells in both the brain and spinal cord. This confirms the selection of the cisterna magna as the injection site and validates that our administered drug can effectively reach the intended target from the cisterna magna.

Second, we administered liposomes loaded with either clodronate or PBS to wildtype rats, forming two distinct groups. The first group received three injections, commencing at day 80 after birth and repeated every 3 weeks, while the second group received a single injection at day 160 after birth. Two weeks after the last injection for the repetitive injection group, all animals were euthanized. Brain and spinal sections were subjected to staining with a CD206 antibody to evaluate the depletion of brain border-associated macrophages. Although CD206-positive cells decreased in all regions, a statistically significant depletion was observed in the spinal cord borders. For the first time, Polfliet et al proposed depletion of BAMs by injecting liposomes containing clodronate locally in 2001. According to them, complete depletion occurs on day seven after injection in the spinal cord and on day ten in the cerebrum. Thereafter, the BAMs begin to repopulate (Polfliet et al., 2001). Since we evaluated the depletion on the tissues collected on the fourteenth post-injection day, we did not end up with complete depletion, but it is worth mentioning that we were able to confirm significant reductions in BAMs in the most important region for ALS investigations, the spinal cord. Hence, we reached our aim of significant depletion at 14th day after injection.

During the experiment, we monitored the weight of the animals twice a week, starting from the injection day until their endpoint. To standardize the data and eliminate gender-related effects, we normalized each animal's weight data to its initially recorded weight. In the single early injection experiment, the depleted group exhibited a higher average weight from the beginning to the symptomatic stage. As the animals began to lose weight, the average weights of the groups converged. In the multiple injection experiment, distinct weight change patterns emerged. From day 80 (the day of the first injection) to approximately 45 days after the last injection (around day 165), the depleted and sham groups exhibited nearly identical average weights. As the symptomatic stage commenced, the depleted animals demonstrated a slower rate of weight loss compared to the sham group. It appears that repetitive doses of clodronate may mitigate weight loss resulting from muscle atrophy. In the single late injection scenario, performed almost before the onset of the symptomatic stage, animals receiving clodronate displayed a higher average weight until one month after the injection. While the sham group entered the symptomatic stage and experienced a decline in average weight, the depleted group maintained their weight. Beyond one-month post-injection, both groups began weight loss at a steeper slope, and the depleted group's average weight eventually matched that of the sham group. In general, it appears that the injection of clodronate could ameliorate muscle atrophy and subsequent weight loss, although the magnitude of this effect varied across the three experiments.

To assess the locomotor activity of the model throughout the experiment duration, we employed a locomotor scoring scale established by Haulcomb et al. and conducted the evaluations on a weekly basis. (Haulcomb et al.). Additionally, we carried out the ladder rung test and scored the animals using the method detailed in the methods chapter.

In the early stages of the single injection experiment, both the depleted and sham groups exhibited similar locomotor scores until the presymptomatic phase. Following the weight decrease and during the symptomatic stage phase, the depleted group experienced a more rapid decline in average scores compared to the sham group. However, during the final weeks of the experiment, the average score of the sham group fell below that of the depleted group. The ladder rung test results for these groups followed a similar trend to the locomotor scores. Following the onset of the symptomatic phase, the depleted group's ladder rung scores declined more rapidly than those of the sham group. Despite the depleted group demonstrating better performance in the ladder rung test at the end of the

experiment, the sham group consistently achieved higher scores in the majority of scoring sessions.

In the multiple injections experiment, the depleted and sham groups initially showed nearly identical average scores until the last injection at the age of 120 days. Following this point, the depleted group consistently exhibited higher average scores in almost all scoring sessions until the conclusion of the experiment. Additionally, during the symptomatic phase, the ladder rung average scores of the depleted group surpassed those of the sham group. However, in the final weeks of the experiment, as all animals approached the endpoint, the average scores of both groups converged. This observation is consistent with the trends in the weight change graphs, where the depleted group's average weight curve declined more gradually than the sham group's after entering the symptomatic phase, and the average scores mirrored this pattern.

Similarly, in the single late injection experiment, the depleted group consistently demonstrated higher average scores compared to the sham group in almost all scoring sessions, with only two exceptions in the middle of the experiment. Their ladder rung scores showed a similar trend. In the initial month post-injection, the depleted group exhibited superior performance on the ladder rung test, but as time progressed, the difference between the groups diminished. Once again, these results align with the patterns observed in the weight change graphs, where a higher average weight corresponded to higher average scores.

To assess the impact of our intervention on group survival and the likelihood of not exhibiting symptoms, we employed the Kaplan-Meier analysis test.

In the single early injection experiment, we found no notable difference in survival between the depleted and sham groups. However, when we defined the peak weight age as the event instead of the termination day, we observed a higher percentage of animals that have not reached the pre-symptomatic stage in the depleted group compared to the sham group. Nevertheless, this difference did not achieve statistical significance (P value = 0.192). This outcome aligns with the higher weight average of the depleted group, suggesting that their larger body mass may contribute to a delayed initiation of weight loss compared to the sham group. This observation is consistent with studies in humans diagnosed with ALS, where a higher BMI correlates with delayed disease onset (Duan et

al., 2023). In summary, the single early dose of clodronate appears to influence the onset of the disease but does not impact overall survival in this context.

The survival test for the multiple injection experiment did not show a significant difference between the depleted and sham groups, despite a slightly higher survival probability in the depleted group (P value = 0.716). However, the probability of animals remaining healthy (not experiencing weight loss) in the depleted group is significantly higher than in the sham group (P value = 0.031). The depleted animals entered the weight loss phase with a significant delay compared to the sham group. These survival data are consistent with the results of neurological tests, where the delayed onset of the weight loss phase aligns with the better locomotor performance observed in the depleted group.

While the survival of the depleted group was initially higher at the beginning of the end stage phase (from the first to the last animal's endpoint) in the single late experiment, the difference in survival probability between the two groups became non-significant as time progressed. Conversely, the second Kaplan-Meier graph for the single late experiment indicates that the likelihood of cases reaching the weight loss phase is higher in the sham group than in the depleted group. In other words, the percentage of animals remaining healthy is higher in the depleted group compared to the sham group (P value = 0.055).

We studied the status of the CD206 positive cells (BAMs), astrocytes, and microglia in the CNS of the rats at the end point of the experiment.

As a result of CD206 IF staining, image analysis reveals upregulation of perivascular macrophages in the ventral horn of lumbar sections of the spinal cord in the depleted group for the multiple injection experiment. The CD206 density in depleted samples was significantly higher than in the sham group, while in the brain cortex and striatum, there was no notable difference. It is interesting that despite a significant reduction of CD206 positive cells in the spinal cord of animals injected with repetitive doses of clodronate-loaded liposomes compared to those injected with PBS-loaded liposomes two weeks after the last injection, by the endpoint, the cells appear to be over-repopulated in the depleted animals. It seems that the depletion of $CD206^{+}$ cells in SOD1 mutated animals leads to a more intense upregulation of these cells after the clodronate effect diminishes. However, it is not studied whether the depletion by clodronate would cause more robust upregulation. The repopulation appears more intense in the multiple injection experiment

compared to the single late injection experiment, because the difference between the depleted and sham groups in the single late injection experiment is not significant. This difference can be explained as follows: the repetitive doses of clodronate have depleted the $CD206^+$ cells more effectively than the single late injection in the beginning; but as the time interval from the injection to the endpoint in the multiple injection is longer than the single late injection experiment, at the endpoint the depleted and sham groups in the single late experiment are not different in $CD206^+$ cells population.

Although we did not study whether the $CD206^+$ cells are of the anti-inflammatory phenotype ($Lyve1^+$) or the pro-inflammatory phenotype ($MHCII^+$), it is reported that the proportion of $MHCII^+$ to $Lyve1^+$ cells is greater at the endpoint of the SOD1 mice compared to WT mice (Adachi et al., 2023). As discussed previously, depleted animals in the multiple injection experiment exhibited slower weight loss and a significantly delayed onset of the presymptomatic phase compared to the sham group. Additionally, they performed better in locomotor activity tests during the symptomatic stage. Based on these observations, we can hypothesize that the overpopulation of $CD206^+$ cells in the multiple depletion group is a result of the activation of the anti-inflammatory phenotype ($Lyve1^+$ $CD206^+$ cells).

To assess astrogliosis, we performed IF staining with the GFAP antibody on the same tissues used for CD206 IF staining. Similarly, GFAP expression was increased in the ventral horn of the lumbar sections of the spinal cord in the multiple depletion group compared to the sham group, while in other regions and in the single late injection experiment, there were no notable differences between the depleted and sham groups. As GFAP is a marker of both anti-inflammatory and pro-inflammatory astrocytes (A2 and A1, respectively (Liddelow et al., 2017)), we cannot conclusively determine the phenotype of the reactivated astrocytes. However, based on the results of behavioral tests and survival data, we can speculate that the increased expression of GFAP may result from the activation of A2 astrocytes in the ventral horn of the multiple depletion animals.

Microglia activation was evaluated through Iba 1 IF staining on similar tissues. Surprisingly, we observed greater microglia activation in the ventral horn of the depleted group compared to the sham group, not only in the multiple injection experiment but also in the single late injection experiment. However, in the brain sections, there was no notable change. Similar to PVMs and astrocytes, microglia activation may be associated with upregulation of the M2 phenotype. As previously discussed, the depleted groups

exhibited better performance in tests, and their weight loss was slower compared to the sham group.

CHAPTER 5

5 Conclusion

A comprehensive investigation has been presented in this thesis project regarding the role of PVMs in ALS in the SOD1$^{(G93A)}$ mutant rat used as a model of ALS. Our study aimed to understand the effect of depleting PVMs by injecting liposomes containing clodronate into the cisterna magna of the animal model of the disease in order to determine the effect on disease progression, weight fluctuations, locomotor activity, and survival rates of the animal model.

We showed that there is a significant difference in the number of border-associated macrophages in SOD1 rats compared to wild-type rats, particularly in the ventral horn and perivascular area of the spinal cord and brain.

A delay in weight loss and an improvement in locomotor performance were observed during the symptomatic stage of ALS when CD206^{+} cells were depleted. The depletion of PVMs, however, had no significant impact on the overall survival of the study subjects.

In addition, the study shed light on the complex interplay between CD206^{+} cells, astrocytes, and microglia in the pathogenesis of ALS. Although PVM depletion initially reduced CD206^{+} cells, subsequent over-repopulation of these cells was observed in the depleted group at the end point of the experiment, when the animals were sacrificed. Considering the higher scores and slower weight loss of the depleted group, this observation may indicate a shift in the PVM phenotype towards an anti-inflammatory one. Activation of microglia and upregulation of astrocytes followed the upregulation of PVMs at the end point of the depleted group. We can also conclude that this upregulation is caused by A2 astrocytes and M2 microglia phenotypes that are anti-inflammatory.

As we observed better results in the multiple injection experiment, we suggest further research in this area. For future studies, increasing the number of injections to deplete the PVMs more effectively is recommended to ensure their population is close to zero at the symptomatic stage.

In general, these findings contribute to a better understanding of the pathogenesis of ALS and indicate that targeting PVMs in the treatment of ALS may have therapeutic

implications. To elucidate the precise mechanisms underlying the involvement of PVMs in ALS, and to explore novel therapeutic approaches aimed at targeting these cells, further research is necessary.

BIBLIOGRAPHY

Adachi, K., Miyata, K., Chida, Y., Hirose, M., Morisaki, Y., Yamanaka, K., & Misawa, H. (2023). Depletion of perivascular macrophages delays ALS disease progression by ameliorating blood-spinal cord barrier impairment in SOD1G93A mice [Original Research]. *Frontiers in Cellular Neuroscience*, *17*. https://doi.org/10.3389/fncel.2023.1291673

Bechmann, I., Kwidzinski, E., Kovac, A. D., Simbürger, E., Horvath, T., Gimsa, U., Dirnagl, U., Priller, J., & Nitsch, R. (2001). Turnover of Rat Brain Perivascular Cells. *Experimental Neurology*, *168*(2), 242-249. https://doi.org/https://doi.org/10.1006/exnr.2000.7618

Beers, D. R., Henkel Js Fau - Xiao, Q., Xiao Q Fau - Zhao, W., Zhao W Fau - Wang, J., Wang J Fau - Yen, A. A., Yen Aa Fau - Siklos, L., Siklos L Fau - McKercher, S. R., McKercher Sr Fau - Appel, S. H., & Appel, S. H. Wild-type microglia extend survival in PU.1 knockout mice with familial amyotrophic lateral sclerosis. (0027-8424 (Print)).

Boillée, S., Yamanaka K Fau - Lobsiger, C. S., Lobsiger Cs Fau - Copeland, N. G., Copeland Ng Fau - Jenkins, N. A., Jenkins Na Fau - Kassiotis, G., Kassiotis G Fau - Kollias, G., Kollias G Fau - Cleveland, D. W., & Cleveland, D. W. Onset and progression in inherited ALS determined by motor neurons and microglia. (1095-9203 (Electronic)).

Bruijn, L. I., Becher Mw Fau - Lee, M. K., Lee Mk Fau - Anderson, K. L., Anderson Kl Fau - Jenkins, N. A., Jenkins Na Fau - Copeland, N. G., Copeland Ng Fau - Sisodia, S. S., Sisodia Ss Fau - Rothstein, J. D., Rothstein Jd Fau - Borchelt, D. R., Borchelt Dr Fau - Price, D. L., Price Dl Fau - Cleveland, D. W., & Cleveland, D. W. ALS-linked SOD1 mutant G85R mediates damage to astrocytes and promotes rapidly progressive disease with SOD1-containing inclusions. (0896-6273 (Print)).

Chiò, A., Logroscino, G., Traynor, B. J., Collins, J., Simeone, J. C., Goldstein, L. A., & White, L. A. (2013). Global epidemiology of amyotrophic lateral sclerosis: a systematic review of the published literature. *Neuroepidemiology*, *41*(2), 118-130. https://doi.org/10.1159/000351153

Clement, A. M., Nguyen Md Fau - Roberts, E. A., Roberts Ea Fau - Garcia, M. L., Garcia Ml Fau - Boillée, S., Boillée S Fau - Rule, M., Rule M Fau - McMahon, A. P., McMahon Ap Fau - Doucette, W., Doucette W Fau - Siwek, D., Siwek D Fau - Ferrante, R. J., Ferrante Rj Fau - Brown, R. H., Jr., Brown Rh Jr Fau - Julien, J. P., Julien Jp Fau - Goldstein, L. S. B., Goldstein Ls Fau - Cleveland, D. W., & Cleveland, D. W. Wild-type nonneuronal cells extend survival of SOD1 mutant motor neurons in ALS mice. (1095-9203 (Electronic)).

Cunha-Oliveira, T., Montezinho, L., Mendes, C., Firuzi, O., Saso, L., Oliveira, P. J., & Silva, F. S. G. (2020). Oxidative Stress in Amyotrophic Lateral Sclerosis: Pathophysiology and Opportunities for Pharmacological Intervention. *Oxid Med Cell Longev*, *2020*, 5021694. https://doi.org/10.1155/2020/5021694

Di Giorgio, F. P., Carrasco, M. A., Siao, M. C., Maniatis, T., & Eggan, K. (2007). Non–cell autonomous effect of glia on motor neurons in an embryonic stem cell–based ALS model. *Nature Neuroscience*, *10*(5), 608-614. https://doi.org/10.1038/nn1885

Duan, Q.-Q., Jiang, Z., Su, W.-M., Gu, X.-J., Wang, H., Cheng, Y.-F., Cao, B., Gao, X., Wang, Y., & Chen, Y.-P. (2023). Risk factors of amyotrophic lateral sclerosis: a global meta-summary [Systematic Review]. *Frontiers in Neuroscience*, *17*. https://doi.org/10.3389/fnins.2023.1177431

Faraco G Fau - Sugiyama, Y., Sugiyama Y Fau - Lane, D., Lane D Fau - Garcia-Bonilla, L., Garcia-Bonilla L Fau - Chang, H., Chang H Fau - Santisteban, M. M., Santisteban Mm Fau - Racchumi, G., Racchumi G Fau - Murphy, M., Murphy M Fau - Van Rooijen, N., Van Rooijen N Fau - Anrather, J., Anrather J Fau - Iadecola, C., & Iadecola, C. Perivascular macrophages mediate the neurovascular and cognitive dysfunction associated with hypertension. (1558-8238 (Electronic)).

Ferraiuolo, L., Meyer, K., Sherwood, T. W., Vick, J., Likhite, S., Frakes, A., Miranda, C. J., Braun, L., Heath, P. R., Pineda, R., Beattie, C. E., Shaw, P. J., Askwith, C. C., McTigue, D., & Kaspar, B. K. Oligodendrocytes contribute to motor neuron death in ALS via SOD1-dependent mechanism. (1091-6490 (Electronic)).

Goldmann, T., Wieghofer, P., Jordão, M. J. C., Prutek, F., Hagemeyer, N., Frenzel, K., Amann, L., Staszewski, O., Kierdorf, K., Krueger, M., Locatelli, G., Hochgerner, H., Zeiser, R., Epelman, S., Geissmann, F., Priller, J., Rossi, F. M. V., Bechmann, I., Kerschensteiner, M., . . . Prinz, M. (2016). Origin, fate and dynamics of macrophages at central nervous system interfaces. *Nature Immunology*, *17*(7), 797-805. https://doi.org/10.1038/ni.3423

Guttenplan, K. A., Weigel, M. K., Adler, D. I., Couthouis, J., Liddelow, S. A., Gitler, A. D., & Barres, B. A. (2020). Knockout of reactive astrocyte activating factors slows disease progression in an ALS mouse model. *Nature Communications*, *11*(1), 3753. https://doi.org/10.1038/s41467-020-17514-9

Guttenplan, K. A., Weigel, M. K., Prakash, P., Wijewardhane, P. R., Hasel, P., Rufen-Blanchette, U., Münch, A. E., Blum, J. A., Fine, J., Neal, M. C., Bruce, K. D., Gitler, A. D., Chopra, G., Liddelow, S. A., & Barres, B. A. (2021). Neurotoxic reactive astrocytes induce cell death via saturated lipids. *Nature*, *599*(7883), 102-107. https://doi.org/10.1038/s41586-021-03960-y

Haulcomb, M. M., Mesnard-Hoaglin, N. A., Batka, R. J., Meadows, R. M., Miller, W. M., McMillan, K. P., Brown, T. J., Sanders, V. M., & Jones, K. J. Identification of B6SJL mSOD1(G93A) mouse subgroups with different disease progression rates. (1096-9861 (Electronic)).

Hawkes, C. A., & McLaurin, J. (2009). Selective targeting of perivascular macrophages for clearance of beta-amyloid in cerebral amyloid angiopathy. *Proceedings of the National Academy of Sciences of the United States of America*, *106*(4), 1261-1266. https://doi.org/10.1073/pnas.0805453106

Howland, D. S., Liu J Fau - She, Y., She Y Fau - Goad, B., Goad B Fau - Maragakis, N. J., Maragakis Nj Fau - Kim, B., Kim B Fau - Erickson, J., Erickson J Fau - Kulik, J., Kulik J Fau - DeVito, L., DeVito L Fau - Psaltis, G., Psaltis G Fau - DeGennaro, L. J., DeGennaro Lj Fau - Cleveland, D. W., Cleveland Dw Fau - Rothstein, J. D., & Rothstein, J. D. Focal loss of the glutamate transporter EAAT2 in a transgenic rat model of SOD1 mutant-mediated amyotrophic lateral sclerosis (ALS). (0027-8424 (Print)).

Iadecola, C. The Neurovascular Unit Coming of Age: A Journey through Neurovascular Coupling in Health and Disease. (1097-4199 (Electronic)).

Jeong, H.-W., Diéguez-Hurtado, R., Arf, H., Song, J., Park, H., Kruse, K., Sorokin, L., & Adams, R. H. (2022). Single-cell transcriptomics reveals functionally specialized vascular endothelium in brain. *eLife*, *11*, e57520. https://doi.org/10.7554/eLife.57520

Koizumi, T., Kerkhofs, D., Mizuno, T., Steinbusch, H. W. M., & Foulquier, S. (2019). Vessel-Associated Immune Cells in Cerebrovascular Diseases: From Perivascular Macrophages to Vessel-Associated Microglia [Mini Review]. *13*. https://doi.org/10.3389/fnins.2019.01291

Liddelow, S. A., Guttenplan, K. A., Clarke, L. E., Bennett, F. C., Bohlen, C. J., Schirmer, L., Bennett, M. L., Münch, A. E., Chung, W.-S., Peterson, T. C., Wilton, D. K., Frouin, A., Napier, B. A., Panicker, N., Kumar, M., Buckwalter, M. S., Rowitch, D. H., Dawson, V. L., Dawson, T. M., . . . Barres, B. A. (2017). Neurotoxic reactive astrocytes are induced by activated microglia. *Nature*, *541*(7638), 481-487. https://doi.org/10.1038/nature21029

Månberg, A., Skene, N., Sanders, F., Trusohamn, M., Remnestål, J., Szczepińska, A., Aksoylu, I. S., Lönnerberg, P., Ebarasi, L., Wouters, S., Lehmann, M., Olofsson, J., von Gohren Antequera, I., Domaniku, A., De Schaepdryver, M., De Vocht, J., Poesen, K., Uhlén, M., Anink, J., . . . Lewandowski, S. A. (2021). Altered perivascular fibroblast activity precedes ALS disease onset. *Nature Medicine*, *27*(4), 640-646. https://doi.org/10.1038/s41591-021-01295-9

McCampbell, A., Cole, T., Wegener, A. J., Tomassy, G. S., Setnicka, A., Farley, B. J., Schoch, K. M., Hoye, M. L., Shabsovich, M., Sun, L., Luo, Y., Zhang, M., Comfort, N., Wang, B., Amacker, J., Thankamony, S., Salzman, D. W., Cudkowicz, M., Graham, D. L., . . . Miller, T. M. Antisense oligonucleotides extend survival and reverse decrement in muscle response in ALS models. (1558-8238 (Electronic)).

Metz, G. A., & Whishaw, I. Q. The ladder rung walking task: a scoring system and its practical application. LID - 1204 [pii] LID - 10.3791/1204 [doi]. (1940-087X (Electronic)).

Nagai, M., Re Db Fau - Nagata, T., Nagata T Fau - Chalazonitis, A., Chalazonitis A Fau - Jessell, T. M., Jessell Tm Fau - Wichterle, H., Wichterle H Fau - Przedborski, S., & Przedborski, S. Astrocytes expressing ALS-linked mutated SOD1 release factors selectively toxic to motor neurons. (1097-6256 (Print)).

Oskarsson, B., Gendron, T. F., & Staff, N. P. Amyotrophic Lateral Sclerosis: An Update for 2018. (1942-5546 (Electronic)).

Park, L., Uekawa, K., Garcia-Bonilla, L., Koizumi, K., Murphy, M., Pistik, R., Younkin, L., Younkin, S., Zhou, P., Carlson, G., Anrather, J., & Iadecola, C. Brain Perivascular Macrophages Initiate the Neurovascular Dysfunction of Alzheimer Aβ Peptides. (1524-4571 (Electronic)).

Pedragosa, J., Salas-Perdomo, A., Gallizioli, M., Cugota, R., Miró-Mur, F., Briansó, F., Justicia, C., Pérez-Asensio, F., Marquez-Kisinousky, L., Urra, X., Gieryng, A., Kaminska, B., Chamorro, A., & Planas, A. A.-O. CNS-border associated macrophages respond to acute ischemic stroke attracting granulocytes and promoting vascular leakage. (2051-5960 (Electronic)).

Pehar, M., Harlan, B. A., Killoy, K. M., & Vargas, M. R. Role and Therapeutic Potential of Astrocytes in Amyotrophic Lateral Sclerosis. (1873-4286 (Electronic)).

Pires, P. W., Girgla, S. S., Moreno, G., McClain, J. L., & Dorrance, A. M. (2014). Tumor necrosis factor-α inhibition attenuates middle cerebral artery remodeling but increases cerebral

ischemic damage in hypertensive rats. *American journal of physiology. Heart and circulatory physiology*, *307*(5), H658-H669. https://doi.org/10.1152/ajpheart.00018.2014

Pizzino, G., Irrera, N., Cucinotta, M., Pallio, G., Mannino, F., Arcoraci, V., Squadrito, F., Altavilla, D., & Bitto, A. (2017). Oxidative Stress: Harms and Benefits for Human Health. *Oxidative Medicine and Cellular Longevity*, *2017*, 8416763. https://doi.org/10.1155/2017/8416763

Polfliet, M. M. J., Goede, P. H., van Kesteren-Hendrikx, E. M. L., van Rooijen, N., Dijkstra, C. D., & van den Berg, T. K. (2001). A method for the selective depletion of perivascular and meningeal macrophages in the central nervous system. *Journal of Neuroimmunology*, *116*(2), 188-195. https://doi.org/https://doi.org/10.1016/S0165-5728(01)00282-X

Rothstein, J. D. (2009). Current hypotheses for the underlying biology of amyotrophic lateral sclerosis [https://doi.org/10.1002/ana.21543]. *Annals of Neurology*, *65*(S1), S3-S9. https://doi.org/https://doi.org/10.1002/ana.21543

Rothstein, J. D., Van Kammen M Fau - Levey, A. I., Levey Ai Fau - Martin, L. J., Martin Lj Fau - Kuncl, R. W., & Kuncl, R. W. Selective loss of glial glutamate transporter GLT-1 in amyotrophic lateral sclerosis. (0364-5134 (Print)).

Siret, C., van Lessen, M., Bavais, J., Jeong, H. W., Reddy Samawar, S. K., Kapupara, K., Wang, S., Simic, M., de Fabritus, L., Tchoghandjian, A., Fallet, M., Huang, H., Sarrazin, S., Sieweke, M. H., Stumm, R., Sorokin, L., Adams, R. H., Schulte-Merker, S., Kiefer, F., & van de Pavert, S. A. (2022). Deciphering the heterogeneity of the Lyve1+ perivascular macrophages in the mouse brain. *Nature Communications*, *13*(1), 7366. https://doi.org/10.1038/s41467-022-35166-9

Wang, L., Gutmann Dh Fau - Roos, R. P., & Roos, R. P. Astrocyte loss of mutant SOD1 delays ALS disease onset and progression in G85R transgenic mice. (1460-2083 (Electronic)).

Yamanaka, K., Boillee S Fau - Roberts, E. A., Roberts Ea Fau - Garcia, M. L., Garcia Ml Fau - McAlonis-Downes, M., McAlonis-Downes M Fau - Mikse, O. R., Mikse Or Fau - Cleveland, D. W., Cleveland Dw Fau - Goldstein, L. S. B., & Goldstein, L. S. Mutant SOD1 in cell types other than motor neurons and oligodendrocytes accelerates onset of disease in ALS mice. (1091-6490 (Electronic)).

Zeisel, A., Muñoz-Manchado Ana, B., Codeluppi, S., Lönnerberg, P., La Manno, G., Juréus, A., Marques, S., Munguba, H., He, L., Betsholtz, C., Rolny, C., Castelo-Branco, G., Hjerling-Leffler, J., & Linnarsson, S. (2015). Cell types in the mouse cortex and hippocampus revealed by single-cell RNA-seq. *Science*, *347*(6226), 1138-1142. https://doi.org/10.1126/science.aaa1934